A Regulatory Loop between the Retinoid-Related Orphan Nuclear Receptor NHR-23 and *let-7* family microRNAs Modulates the *C. elegans* Molting Cycle

Ruhi Patel[1] and Alison R. Frand[1]*

[1]Department of Biological Chemistry
David Geffen School of Medicine
University of California, Los Angeles
Los Angeles, CA 90095

*To whom correspondence should be addressed: afrand@mednet.ucla.edu

Keywords: circadian clocks, developmental timers, behavioral quiescence (sleep), oscillatory gene expression, *Period*, *Per2*, *lin-42*

32 **Abbreviations:**

33

34 UTR	Untranslated Region
35 RNA	Ribonucleic Acid
36 RNAi	RNA interference
37 ROR	Retinoid-related Orphan Receptor
38 HRE	Hormone Response Element
39 NHR	Nuclear Hormone Receptor
40 PER	PERIOD gene
41 GFP	Green Fluorescent Protein
42 iCLIP	Individual-nucleotide resolution Crosslinking Immunoprecipitation
43 RORE	ROR Response Element
44 LCS	*let-7* consensus site
45 NHR	Nuclear Hormone Receptor
46 Mlt	Molting Cycle Defective
47 MFE	Minimum Free Energy
48 pri	Primary
49 Let	Lethal
50 CRISPR	Clustered Regularly Interspersed Short Palindromic Repeats
51 crRNA	CRISPR RNA
52 tracrRNA	Trans-activating crRNA
53 nt	Nucleotides
54 td	Tandem
55 ssODN	Single Stranded Oligodeoxynucleotides
56 VPC	Vulval Precursor Cell

57

SUMMARY

Animal physiology and development both rely on biological clocks, but the extent to which feedback loops among core components of the circadian clock and conserved microRNAs operate within developmental timers is not well understood. Here, we show that a negative feedback loop between NHR-23/RORα and *let-7* modulates the PER-dependent rhythm of the *C. elegans* molting cycle. Related quiescent intervals are delayed and protracted in *nhr-23* knockdowns, advanced and abbreviated in particular *let-7* mutants, and yet scheduled more regularly in double mutants. NHR-23 binds upstream ROR Response Elements (REs) and activates transcription of primary *let-7* when larvae are active, whereas *let-7* targets an LCS in the 3′UTR and represses expression of *nhr-23* transcripts when larvae are quiescent. Moreover, NHR-23 and *let-7* have scores of shared targets that are cyclically expressed and mediate related transitions in cell and animal behavior. ROREs are also found upstream of vertebrate *let-7* homologs, while LCSs are found in 3′UTRs of *ROR* transcripts. Conservation of this feedback loop has implications for human clocks and related malignancies and disorders of sleep and metabolism.

INTRODUCTION

Timekeeping and time management are biological imperatives. Distinct timers govern key features of rhythmic events during development such as the time interval between each event and the number of times the event is repeated. Some examples are the developmental timers that regulate the segmentation of insects and the formation (and segmentation) of vertebrate somites (El-Sherif et al., 2012; Gomez et al., 2008). Mutations that affect principal components of the somitogenesis clock can cause neonatal mortality (Matsu-Ura et al., 2016; Sparrow et al., 2007).

The circadian clock, which coordinates sleep-wake cycles and other physiologic rhythms with the solar day, is perhaps the best-characterized biological timer. Moreover, core components of the circadian clock, such as PERIOD, also regulate behavioral and seasonal rhythms — the periods of these rhythms range from milliseconds to months. Mutations that affect core components of the circadian clock cause acute sleep disorders, metabolic syndromes, and malignancies, underscoring the significance of the circadian clock to human health (Oyama et al., 2017; Patke et al., 2017; Puram et al., 2016; Roenneberg and Merrow, 2016).

Interconnected positive and negative transcriptional–translational feedback loops (TTFLs) are the mainstay of clock biology (Takahashi, 2016). The transcriptional activators CLOCK and BMAL1 and their repressor PERIOD are core components of the circadian clock. Retinoid-Related Orphan Receptors (ROR) activate the expression of *BMAL1*, integrating organ-specific and CNS clocks (Cook et al., 2015; Zhang et al., 2017). Recent studies have uncovered microRNA-mediated, post-transcriptional feedback loops that modulate the circadian clocks of peripheral tissues. The breadth and significance of these regulatory loops to the assortment of physiologic and developmental timers remain unclear.

PER proteins also regulate the molting cycles of both arthropods and nematodes (Olmedo et al., 2017). *C. elegans* molt 4 times at regular intervals, once every 8–10 h under typical culture conditions. The process of molting involves separation of the existing cuticle from the epidermis (apolysis) and replacement with a larger cuticle for the upcoming life stage. Episodes of behavioral quiescence (lethargus) accompany renovation of the integument and last 2–3 h. Lethargus is now considered a model for sleep based on shared features such as neuroendocrine regulation, sensory depression and homeostatic drive (Trojanowski and Raizen, 2016).

107 Finding that LIN-42, the *C. elegans* counterpart of insect and mammalian *Period*,
108 is required for worms to molt at regular intervals implied the existence of a molting cycle
109 timer ancestrally related to the circadian clock (Jeon et al., 1999; Monsalve et al., 2011).
110 Levels of *lin-42* transcripts cycle in time with the molts, as do levels of this
111 transcriptional repressor seen in the nucleus. Additional components of the molting
112 timer – especially regulators of gene expression – were anticipated but not identified.
113 One candidate was the orphan nuclear hormone receptor NHR-23, the one and
114 only worm homolog of vertebrate RORs (Antebi, 2015). The *nhr-23* gene itself is
115 required for completion of the molts and is transiently but repeatedly expressed in the
116 epidermis during each larval stage. Moreover, NHR-23 directly or indirectly promotes
117 the expression of many downstream targets linked to the molting process. (Frand et al.,
118 2005; Kouns et al., 2011).
119 The *let-7* family of miRNAs (hereafter *"let-7s"*) were also logical candidates for
120 components of the molting cycle timer. Historically, the *let-7* gene was first
121 characterized during studies of the heterochronic pathway, which specifies successive
122 temporal fates manifest by the epidermal stem (seam) cells of *C. elegans* (Ambros and
123 Ruvkun, 2018; Reinhart et al., 2000). The *let-7* miRNA promotes the larval-to-adult
124 transition, while the paralogs *mir-48* and *mir-241* together specify the L2 fate (Abbott et
125 al., 2005). A third paralog, *mir-84,* appears to act cooperatively with *let-7*, *mir-48,* and
126 *mir-241* across development. The *let-7s* are recognized effectors of the number of molts
127 but not the pace of the molting cycle. However, primary *let-7s* transcripts are cyclically
128 expressed in phase with the molts in the seam cells, which repeatedly alternate
129 between division and quiescence in coordination with the molting cycle (Van
130 Wynsberghe et al., 2011).
131 Genetic interactions among NHR-23, let-7, and LIN-42 were uncovered in prior
132 studies. Specifically, *let-7* suppresses supernumerary molts by directly or indirectly
133 repressing both *nhr-23* and *nhr-25*, which is a homolog of SF-1 (Hayes et al., 2006).
134 Moreover, a feedback loop between *lin-42/Per* and *let-7 was* uncovered by co-
135 suppression of heterochronic phenotypes and further molecular analyses (McCulloch
136 and Rougvie, 2014; Perales et al., 2014; Van Wynsberghe et al., 2014). The extent, if
137 any, to which the abovementioned interactions affect the biorhythm of molting was not
138 clear.

139 Here, we show that both *nhr-23* and *let-7s* modulate the biorhythm of molting,
140 exerting opposing but co-dependent effects on the pace of larval development.
141 Explicating this, we show that NHR-23 activates expression from the promoter of *let-7*,
142 whereas *let-7s* dampen the pulsatile expression of *nhr-23* transcripts from the L2 stage
143 through adulthood. Further, we identify scores of shared targets of both NHR-23 and
144 *let*-7s, each of which is cyclically expressed and linked to the process of molting.
145 Evidence that the feedback loop between NHR-23/RORα and *let-7s* is conserved in
146 vertebrates has clear implications for human clocks and related malignancies along with
147 disorders of sleep and metabolism.
148
149 **RESULTS**
150 **Opposite effects of *nhr-23* and *let-7s* modulate the biorhythm of molting.**
151 Newly hatched *C. elegans* larvae undergo four molts at regular 8-10 h intervals
152 prior to emergence in the adult stage (Figure 1A). As such, L1 larvae simultaneously
153 released from starvation-induced diapause and cultivated with food subsequently
154 complete the molts in concert. To quantify and compare the biorhythms of selected
155 strains versus wild-type *C. elegans* (N2), we systematically observed individual worms
156 at regular 1 h intervals, videotaping for 15 s on the hour. The subjects composed
157 isogenic cohorts developing from the 2nd to 3rd larval stage (L2 to L3), from the 3rd to the
158 4th larval stage (L4), and from the 4th larval stage to adulthood. Active worms were
159 identified by locomotive (sinusoidal) body movements and pharyngeal muscle
160 contractions (pumps). Recorded frequencies of pumps were measured *post hoc* and
161 graded as high, medium, or low on a scale set by the mean and standard deviation of
162 age-matched, wild-type worms. Lethargic worms were identified by the absence of
163 detectable pumps or locomotion, combined with a rectilinear or hockey stick-like body
164 posture (Iwanir et al., 2013; Raizen et al., 2008). Separation of the preexisting cuticle
165 from the body and detection of its remnants on the culture plate signified the
166 commencement and completion of ecdysis (Singh and Sulston, 1978).
167 The actograms in Figure 1B display records from key longitudinal studies in
168 reverse chronological order. As anticipated, cohorts of wild-type larvae passed through
169 active and lethargic intervals practically in sync. For instance, wild-type animals were
170 active for 8.1 ± 0.5 h (mean ± sd) during L4 and lethargic for 2.2 ± 0.4 h during the
171 L4/adult molt. Afterward, wild-type adults escaped from the outmoded cuticle and

172 quickly recommenced the abovementioned activities. Supplemental Table 1 specifies
173 both the active and lethargic interval along with the wake-to-wake interval — defined as
174 the time elapsed between two chronological transitions from dormancy to activity — for
175 each experimental cohort.

176 To evaluate the potential regulatory role of NHR-23, we used bacterial-mediated
177 RNA-interference (RNAi) to knockdown *nhr-23* in larvae (Timmons et al., 2001).
178 Rescheduling the initial delivery of *nhr-23* siRNAs circumvented larval arrest and
179 lethality prior to the stage of interest. For example, to observe *nhr-23* knockdowns
180 during L4, hatchlings were cultivated on mock bacteria for 14 h and then transferred to
181 bacteria that expressed *nhr-23* dsRNAs. In addition, only larvae that completed the
182 L3/L4 molt were included in the longitudinal study (see STAR Methods). Following this
183 regimen, all *nhr-23(RNAi)* larvae appeared superficially normal at the start, but none
184 had fully shed the outmoded larval cuticle at the end of the experiment (the Mlt or
185 Molting defective phenotype).

186 L4-stage *nhr-23(RNAi)* animals were active ~20 min longer and lethargic 2.4 ± 0.8 h
187 longer than mock-treated wild-type animals. L3-stage *nhr-23(RNAi)* larvae were active
188 1.4 ± 1.3 h longer and lethargic 2.2 ± 1.9 h longer than control animals (Figure 1B′). In
189 this study, one *nhr-23(RNAi)* larva was quiescent during 9 consecutive time samples.
190 An L2-stage cohort of *nhr-23(RNAi)* larvae was lethargic for 2.6 ± 1.2 h longer than wild-
191 type larvae. This lengthy delay coincided with the most potent knockdown of *nhr-23*, as
192 indicated by qRT-PCR (see STAR Methods). Thus, delayed and protracted sleep-like
193 phases were associated with knockdown of *nhr-23* during three successive life stages.

194 The majority of *nhr-23(RNAi)* animals also appeared sluggish after awakening from
195 lethargus. In principle, incomplete remodeling of the pharyngeal cuticle could account
196 for diminished pumping rates. Alternatively, knockdown of *nhr-23* could lead to less
197 robust and/or irreversible transitions from quiescence to activity.

198 To determine whether *let-7s* also regulate the biorhythm of molting, we tracked
199 cohorts of both *let-7(n2853)* and *let-7(mg279)* animals using the same approach. Both
200 mutations are associated with lower levels of mature *let*-7 relative to wild type. However,
201 *n2853* is a substitution in the seed sequence, whereas *mg279* is a 27-bp deletion
202 upstream of the mature miRNA (Bracht et al., 2004; Reinhart et al., 2000). The cohort of
203 *let-7(n2853)* animals progressing from L4 to adulthood entered lethargus 1.8 ± 0.6 h
204 earlier and reawakened 0.7 ± 0.6 h faster than wild-type animals (Figure 1B). A distinct

205 L4 cohort of *let-7(n2853)* animals isolated from a second strain also developed faster. In
206 both experiments, *let-7(n2853)* animals ruptured 1 to 6 h after ecdysis—a hallmark of
207 strong loss-of-function alleles caused by abnormal morphogenesis of the vulva (Ecsedi
208 et al., 2015). The cohort of *let-7(n2853)* larvae progressing from L3 to L4 became
209 lethargic 0.7 ± 0.7 h earlier and reawakened ~0.3 h faster than wild-type animals (Figure
210 1B′). All but one *let-7(n2853)* worm went on to complete the subsequent molt —
211 outpacing the entire wild-type cohort. Cohorts of *let-7(mg279)* single and *let-7(mg279)*
212 *mir-84(tm1304)* double mutants progressing from L4 to adulthood became lethargic 0.6
213 ± 0.8 h and 1.7 ± 1 h earlier than wild-type animals, respectively (Supplemental Table
214 1). Thus, advanced sleep-like phases were recorded in three distinct *let-7(-)* strains, all
215 of which developed faster than wild-type larvae.

216 To further characterize genetic interactions between let-7 and NHR-23 relevant to
217 the pace of the molting cycle, we combined *let-7(n2853)* with stage-restricted
218 *nhr-23(RNAi)* and tracked the resulting animals (Figure 1B and 1B′). Both the L4- and
219 the L3-stage cohorts of *nhr-23(RNAi) let-7(n2853)* double mutants remained active
220 longer than *let-7(n2853)* single mutants and reawakened faster than *nhr-23(RNAi)*
221 single mutants, indicating that changes in the biorhythm associated with each single
222 mutant were partially co-suppressed. The corresponding wake-to-wake intervals of
223 *nhr-23(RNAi)* single knockdowns, *let-7(n2853)* single mutants, *nhr-23(RNAi) let-*
224 *7(n2853)* double mutants, and wild-type animals progressing from L4 to adulthood were:
225 13.1 ± 1 h, 7.9 ± 0.6 h, 10.6 ± 0.8 h, and 10.3 ± 0.5 h, respectively. A similar trend was
226 observed across the L3-to-L4 molt. Moreover, a triple knockout of the *let-7* sisters
227 partially suppressed the prolonged lethargus caused by RNAi of *nhr-23* during the L2
228 stage (Supplemental Table 1). RNAi of *nhr-23* also suppressed the rupture of
229 *let-7(n2853)* animals, possibly because NHR-23 normally binds the promoter and
230 activates expression of *lin-41*, the key target of *let-7* germane to integrity of the vulva
231 (Celniker et al., 2009; Ecsedi et al., 2015). Together, findings from the longitudinal
232 studies suggest that feedback among *nhr-23* and *let-7s* modulates the biorhythm of
233 molting.

234 Considering the abovementioned phenotypes and prior studies of *lin-42* (Edelman et
235 al., 2016; Monsalve et al., 2011), it seems that LIN-42 may be the shared target at the
236 nexus—all three compose the core oscillator. Consistent with this model, NHR-23
237 occupies the distinct promoters of *lin-42a* and *lin-42b/c in vivo* (Celniker et al., 2009).

238 Moreover, knockdown of *nhr-23* during the L4 stage abrogated the corresponding pulse
239 in expression of *lin-42* (Supplemental Figure 1). Findings are consistent with the model
240 that NHR-23 and *let-7s* act in opposing limbs of the molting timer, together with
241 LIN-42/PER.
242
243 **NHR-23 Binds and Repeatedly Activates the Promoter of *let-7*.**
244 One molecular model consistent with the abovementioned results is that NHR-23
245 directly activates the transcription of primary *let-7*, whereas *let-7* represses the
246 expression of *nhr-23* transcripts. Both ROR and NHR-23 monomers bind the core
247 response element (RORE) 5′-(A/G)GGTCA-3′ to activate gene expression
248 (Kostrouchova et al., 1998; Ueda et al., 2002). Computational searches identified three
249 ROREs within the minimal promoter of *let-7* (Figure 2A), which is necessary and
250 sufficient for robust expression in the epidermis (Johnson et al., 2003). NHR-23
251 evidently occupies a ~300bp region aligned with the RORE cluster *in vivo* (Celniker et
252 al., 2009). NHR-23 also occupies ROREs identified in the upstream regulatory regions
253 of all three *let-7* sisters (Supplemental Table 3).
254 To determine the extent to which NHR-23 activates the *let-7* promoter, we
255 compared the expression of a *let-7p::nls-gfp* transcriptional reporter (Kai et al., 2013) in
256 stage-restricted *nhr-23(RNAi)* and mock-treated animals via quantitative fluorescence
257 microscopy. Beforehand, we measured the intensity of GFP in epidermal nuclei of
258 transgenic animals developing from L3 into adults. GFP was barely detectable early in
259 L3 and L4, but the signal intensified throughout both stages and peaked during the
260 subsequent molts (data not shown). Accordingly, transgenic animals were imaged early
261 in the L3/L4 and L4/A molts (Figure 2B and 2C). At both stages, the signal intensity in
262 hyp7 nuclei was 2.3 ± 1.3-times (mean ± SD) lower in *nhr-23(RNAi)* than mock-treated
263 animals. Levels of GFP in seam nuclei were more variable during the L3/L4 than the
264 L4/A molt, possibly due to continuation of the cell cycle. Even so, the average signal
265 intensity in the seam was lower in *nhr-23* knockdowns than mock-treated animals during
266 both molts.
267 As a complementary approach, we used TaqMan qRT-PCR to measure and
268 compare the levels of both primary *let-7* transcripts and mature *let-7* in L4-restricted
269 *nhr-23(RNAi)* versus mock-treated, wild-type animals. For this purpose, we collected
270 and processed regular 2-h time samples of synchronized populations developing from

271 L3 to adulthood. Comparable levels of pri-*let-7* were initially detected in both cohorts
272 (Figure 2D). Levels of pri-*let-7* detected in mock-treated animals peaked at mid-L4 —
273 4.6 times higher than the preceding trough. In contrast, pri-*let-7* levels either decreased
274 or marginally increased in comparable time samples of *nhr-23(RNAi)* animals.
275 Furthermore, levels of mature *let-7* detected in both mock-treated and *nhr-23(RNAi)*
276 animals initially increased during the L3 stage (Figure 2E). However, levels of *let-7* in
277 mock-treated animals increased by another 160% across the L4 stage and L4/A molt,
278 whereas levels of mature *let-7* stagnated in *nhr-23(RNAi)* animals, even though only
279 35% of *nhr-23(RNAi)* animals were observed to be molting defective under the
280 experimental conditions. Molting-defective larvae were first observed as levels of *let-7*
281 plateaued, consistent with the attribution of both phenotypes to the knockdown of
282 *nhr-23*. Thus, both pulsatile expression of pri-*let-7* and accretion of mature *let-7* partly
283 depend on the function of *nhr-23.*
284
285 **The 3′UTR of *nhr-23* contains a repressive element complementary to *let-7.***
286 We next asked whether *let-7*-family miRNAs target *nhr-23* transcripts in
287 developing larvae. Direct inspection of the 868-bp 3′UTR identified four sites partly
288 complementary to *let-7s* (Mangone et al., 2010). One – hereafter, the *let-7* consensus
289 site (LCS) – perfectly complements the 5′ seed region (Figure 3A and Supplemental
290 Table 2). To test the function of these sites, we constructed a suite of bicistronic
291 reporters for post-transcriptional, *cis*-regulatory elements that were housed in
292 extrachromosomal arrays and expressed in transgenic strains (Figure 3B). Briefly, the
293 coding sequence of tandem (td) tomato was fused with the 3′UTR of interest, while the
294 coding sequence of GFP was fused with the 3′UTR of *unc-54*, which is not targeted by
295 *let-7s.* An SL2 trans-splice site bridged the two fusion genes. The promoter of *dpy-7*
296 drove expression of the operon in the hypodermis. Transgenic animals were imaged
297 during the L4/A molt, when both *dpy-7* and mature *let-7* are highly expressed in the
298 epidermis (Figure 3C). Signals from tdTomato were quantified and normalized to signals
299 from GFP within each worm (Figure 3D and 3E). This approach controlled for potential
300 differences in gene expression associated with particular arrays or mosaic animals,
301 rather than the test 3′UTR combined with *tdtomato*.
302 The 3′UTRs of *unc-54* and *lin-41* were cloned into bicistronic reporters used as
303 negative and positive controls, respectively (Vella et al., 2004). Levels of tdTomato were

304 conspicuously higher when combined with the 3′UTR of *unc-54,* rather than the 3′UTR
305 of *lin-41*. The corresponding ratiometric (tdTomato/GFP) values were 2.31 ± 0.32 and
306 0.68 ± 0.19 (mean ± SD). The observed value of 2.3 approached the predicted value of
307 2.4 for the negative control. This similarity corroborated two presuppositions: 1) that
308 trans-splicing would be nearly 100% effective, and 2) that tdTomato and GFP would
309 have nearly equivalent half-lives in vivo (Supplemental Figure 2).
310 Normalized levels of tdTomato were 5.7-times lower when combined with the
311 3′UTR of *nhr-23*, rather than *unc-54.* Any difference in the efficacy of trans-splicing or
312 nonsense-mediated decay of pre-mRNAs could not account for the apparent repression
313 of tdTomato, as no significant difference was detected in the absolute intensity of GFP
314 expressed from either bicistronic reporter (1076 ± 704 a.u. versus 829 ± 392 a.u.,
315 respectively). To identify the specific repressive elements(s), we systematically excised
316 each of the four sites partially complementary to *let-7* from the full-length 3′UTR of
317 *nhr-23*, generating four additional bicistronic reporters. Excision of the LCS led to a two-
318 fold increase in the ratio of tdTomato/GFP signals, relative to the average ratio (0.40 ±
319 0.10) associated with the unaltered reporter for the 3′UTR of *nhr-23* (Figure 3E).
320 Shortening the 3′UTR could not explain the de-repression of tdTomato, considering that
321 three similar 21-nt deletions led to customary or lower levels of tdTomato, as compared
322 with same-day controls. Thus, the 3′UTR of *nhr-23* contains a functional LCS, consistent
323 with the model that *let-7s* bind and repress the expression of *nhr-23* transcripts during
324 the fourth molt and possibly earlier molts as well.
325
326 ***let-7* dampens the expression of *nhr-23* and the shared target *mlt-10.***
327 We next sought to characterize the relationship between *let-7s* and the oscillatory
328 expression of *nhr-23* during larval development. For this reason, we used CRISPR/cas9
329 technology to precisely excise the 21-nt LCS from the endogenous *nhr-23* locus (Paix et
330 al., 2015). The resulting allele – *nhr-23(aaa20)* – was out-crossed to the standard N2
331 strain 3 times. Thereafter we collected *let-7(n2853)*, wild-type, and *nhr-23(aaa20)*
332 samples of ~1,500 worms at regular 2 h intervals—22-50 h after synchronized
333 hatchlings were released from starvation and cultivated on food. RNA was extracted
334 from each sample and the relative abundance of *nhr-23* transcripts determined by
335 TaqMan qRT-PCR (Figure 4A). Anticipating that these three strains might develop at
336 different rates, we counted pumping versus non-pumping worms before collecting each

337 sample. Lethargic phases were subsequently identified by troughs in the proportion of
338 pumping animals. Related graphs include 14 time samples encompassing three
339 lethargic and two active phases per strain.

340 Levels of *nhr-23* transcripts waxed and waned as each cohort progressed from
341 L2 to adulthood (Figure 4A and Supplemental Figure 3A). Peaks were detected ~one-
342 third of the way through L2, L3, and L4 in wild-type samples; however, the amplitude
343 declined from one stage to the next, indicative of dampening. Sharper peaks and wider
344 troughs were detected in *let-7(n2853)* animals. Indeed, the curve was ~5-fold steeper,
345 and the amplitude edged upward in successive developmental stages. Moreover, an
346 extra pulse of *nhr-23* expression was detected in *let-7(n2853)* samples, consistent with
347 the onset of a supernumerary molt. Consequently, *nhr-23* transcripts were ~4.8 times
348 more abundant in *let-7(n2853)* than wild-type young adults. Likewise, the expression
349 curve for *nhr-23* was ~3-fold steeper, and the peaks were 1.7 times higher in
350 *nhr-23*(*aaa20)* mutants, as compared with wild-type animals (Figure 4A′). With the extra
351 pulse, *nhr-23* transcripts were ~3.2 times more abundant in *nhr-23(aaa20)* than wild-
352 type adults. An independent trial produced similar results (Supplemental Figure 3A).

353 We went on to compare the abundance of *nhr-23* transcripts in successive time
354 samples of *mir-241(*Δ*) mir-48(*Δ*) mir-84(n4037)* triple knockouts, *nhr-23(aaa20)* single
355 mutants, and wild-type larvae developing through two lethargic and one active phase —
356 corresponding to L2 (Supplemental Figure 3B). The curves associated with the triple
357 knockout and *nhr-23(aaa20)* were 3 times steeper and, on average, 2.2 times higher in
358 amplitude than the curve seen in wild-type animals. Thus, *let-7* and its paralogs
359 normally restrain the ascent of *nhr-23* transcript levels from the L2 stage through
360 adulthood. Moreover, the LCS functions as a repressive element in physiologic context.
361 Consistent with this finding, ALG-1 is associated with the 3′UTR of *nhr-23* transcripts, as
362 shown by iCLIP Sequencing studies (Supplemental Table 3).

363 To determine the effect of *let-7(n2853)* and the related deregulation of *nhr-23* on
364 the cyclical expression of a downstream gene directly involved in the process of molting,
365 we further quantified *mlt-10* transcripts in the same time samples (Figure 4B). The
366 *mlt-10* gene encodes the founding member of an unconventional family of apical matrix
367 proteins present in all 5 stage-specific cuticles (Meli et al., 2010). The expression curve
368 for *mlt-10* was 4 times steeper and the peaks 1.8 times higher, on average, in samples
369 of both *let-7(n2853)* and *nhr-23(aaa20)* mutants, as compared with wild-type animals. In

370 principle, a supernumerary pulse of *mlt-10* expression might have been detected in
371 *let-7(n2853)* and/or *nhr-23(aaa20)* samples collected more than 50 h after release from
372 L1-diapause. As we describe, *mlt-10* is a shared target of both NHR-23 and *let-7*. As
373 such, *let-7* probably dampens its expression by directly targeting *mlt-10* transcripts and
374 also by targeting *nhr-23* transcripts.

375 How typical is the combination of transcriptional activation by NHR-23 and
376 post-transcriptional repression by *let-7s* among genes linked to the molting cycle? To
377 address this topic, we systematically classified 70 such genes as targets of NHR-23,
378 *let*-7s, both, or neither using bioinformatic approaches and meta-analyses of large data
379 sets. Genes classified as targets of NHR-23 met two of these three criteria: 1) NHR-23
380 occupied the upstream regulatory region *in vivo* (Celniker et al., 2009), 2) more ROREs
381 were found in regulatory regions than explicable by chance, and 3) inactivation of
382 *nhr-23* led to lower transcript levels, as detected by comparative microarrays (Kouns et
383 al., 2011). Genes classified as targets of *let-7s* met these two criteria: More LCSs were
384 found in the 3'UTR of corresponding transcripts than explicable by chance, and the
385 Argonaute protein ALG-1 bound the 3′UTR in vivo, as detected by iClip (Broughton et
386 al., 2016). By these rubrics, 57% (40/70) of the genes linked to molting were identified
387 as shared targets of both NHR-23s and *let-7s*. Among these shared targets, 88% were
388 previously found to be expressed in cycles with an ~8 h frequency in developing larvae
389 (Hendriks et al., 2014; Kim et al., 2013). In contrast, only 10% (2/20) of randomly
390 selected genes with no known link to molting were identified as shared targets (Figure
391 4C, Supplemental Table 3). Evidently, joint regulation by NHR-23 and *let-7s* is a
392 signature of protein-coding genes that are both associated with the molting cycle and
393 expressed in correlated waves.

394 Is the feedback loop between NHR-23/RORα and *let-7s* conserved between nematodes
395 and vertebrates? Using bioinformatic approaches, we identified multiple ROREs
396 upstream of *let-7* homologs annotated in the genomes of humans, mice, and zebrafish.
397 For example, 4-5 ROREs were identified upstream of mammalian *let-7-a*; at most, 3 of
398 these 6-mers could be explained by chance alone (Supplemental Figure 4A). Moreover,
399 we identified multiple LCSs in the 3′UTRs of *ROR* transcripts annotated in the genomes
400 of zebrafish and mammals. Four sites partially complementary to *let-7* were uncovered
401 in the 3′UTR of human RORα – one of which perfectly matched the *let-7* seed
402 (Supplemental Figure 4B). Furthermore, by inspecting the regulatory sequences of

403 human *PER2*, we identified one RORE upstream of the transcriptional start site and two
404 LCSs in the 3′UTR of *Per2* transcripts. The apparent conservation of these cis-
405 regulatory elements suggests that similar feedback loops among RORα, *let-7s,* and
406 PER2 may modulate the expression of all three genes in human tissues.
407
408 **DISCUSSION**
409 The key findings of this report formulate a refined model for the molting timer
410 (Figure 4D-F). Therein, NHR-23/RORα transcriptionally activates *let-7,* the *let-7* sisters
411 and *lin-42/per*, which represses the expression of pri-*let-7* (McCulloch and Rougvie,
412 2014; Perales et al., 2014; Van Wynsberghe et al., 2014). The *let-7*-family post-
413 transcriptionally represses both *nhr-23* and *lin-42*. This set of regulatory interactions
414 compose interconnected positive and negative feedback loops with time delays — the
415 essential framework of biological clocks. In the proposed model, intrinsic differences
416 between the rates of protein versus miRNA biogenesis influence the time intervals
417 needed for levels of NHR-23, LIN-42, and *let-7s* to rise from troughs to effective
418 concentrations.
419 The proposed mechanism accounts for the relative phases and shapes of the
420 expression curves of *nhr*-23 and *let*-7 observed in wild-type animals. As described, peak
421 levels of *nhr-23* decrease through successive larval stages (Figure 4A). Nevertheless,
422 levels of NHR-23 reach 50% of the stage-specific peak early in each stage. However,
423 levels of primary *let-7* reach the same threshold halfway through each larval stage
424 (Figure 4E). This difference – 1.6 h under our experimental conditions – is consistent
425 with activation of the *let-7* promoter by NHR-23 (Figure 4F). In addition, levels of both
426 *nhr-23* transcripts and proteins peak one-third of the way through each larval stage;
427 thereafter, levels of *nhr-23* transcripts descend more rapidly than levels of NHR-23
428 fusion proteins, consistent with miRNA-mediated degradation and/or translational
429 inhibition. Levels of *lin-42* transcripts peak around the same time, if not later than levels
430 of pri-*let-7* (Supplemental Figure 1B).
431 Inflections in the expression curves of NHR-23 and *let-7* further relate to
432 recurrent events in the molting cycle. In the positive limb of the timer, NHR-23 levels
433 ascend as animals commit to a forthcoming molt. In the negative limb of the timer, *let-7s*
434 repress the expression of *nhr-23* and NHR-23 levels fall as animals transit the molt. This
435 repression decelerates the accrual of NHR-23 in the next life stage and delays the onset

436 of any subsequent molt. Consistent with this model, *let-7(n2853)* mutants were
437 associated with both the steeper ascent of *nhr-23* transcripts and earlier onset of the
438 lethargic phase at the end of L4.

439 In theory, even small differences in the threshold concentrations of core
440 components needed to regulate specific downstream targets could enable a single timer
441 to illicit orderly waves in the expression of distinct sets of proteins that mediate
442 sequential transitions or events in the molting cycle. For example, the molting timer
443 could control both the onset and termination of lethargus by regulating both
444 sleep-promoting peptides such as *osm-11* and *flp-13* and wake-promoting peptides
445 such as *flp-2* and *pdf-1* (Chen et al., 2016; Nelson et al., 2014; Singh et al., 2011).
446 Other timer-controlled genes encode proteins involved in tissue renovation, such as
447 *mlt-10* (Meli et al., 2010).

448 The concept that levels of both NHR-23 and *let-7s* must reach target-specific
449 thresholds to effectively promote or repress gene expression is supported by particular
450 findings in this report and also by current knowledge in the fields of gene regulation and
451 chronobiology (Antebi, 2015; Takahashi, 2017). Indeed, the capacity of NHR-23 to
452 activate any specific target might depend on its concentration relative to the number of
453 functional ROREs in the target promoter; the abundance of co-activators, co-repressors,
454 and competitive NHRs; and the availability of as-yet unidentified ligand(s) derived from
455 dietary steroids or exogenous cholesterol (Galles et al., 2018; Santori et al., 2015). The
456 capacity of *let-7s* to silence any specific target might depend on the number of LCSs
457 within the 3′UTR; the abundance of cooperative miRNAs, and the availability of
458 processing factors or RISC components such as Dicer and ALG-1, respectively. Many
459 of these factors change in predictable ways over time, adding layers of complexity to the
460 timing machinery.

461 The duration of each larval stage and the total number of molts may be
462 integrated at the level of expression of *nhr-23*. In wild type animals, which undergo 4
463 molts, peak levels of *nhr-23* transcripts dampen from the L1 to the L4 stage; the
464 transcripts are no longer detected in adults. In contrast, in *let-7* mutants, which undergo
465 supernumerary molts, the levels of *nhr-23* transcripts do not dampen throughout
466 development and a supernumerary pulse of *nhr-23* expression is detected in adults.
467 Expression of *nhr-23* in *let-7* mutant adults is necessary for the oncoming

468 supernumerary molt (Hayes et al., 2006). Thus, dampening of *nhr-23* levels depends on
469 *let-7s* and may count down the total number of molts.

470 Our findings are consistent with the emerging concept that miRNA-mediated
471 feedback loops increase the robustness of numerous gene regulatory networks and
472 related outcomes, including cell fate decisions, stress responses, and developmental
473 trajectories. In one prominent example, ligand-bound molecules of the *C. elegans*
474 nuclear hormone receptor DAF-12 directly enhance and expedite the expression of
475 *let-7*-family miRNAs, whereas *let-7s* directly repress the expression of DAF-12. These
476 events promote continuous development in favorable environments rather than L3-
477 stage diapause (Bethke et al., 2009; Hammell et al., 2009). Another feedback loop
478 wherein the FOXO transcription factor DAF-16 targets mir-34 and vice versa reinforces
479 the commitment to diapause in response to stressors, including sleep deprivation
480 (Driver et al., 2013; Isik et al., 2016).

481 This study recognizes and further integrates miRNA-mediated feedback loops
482 within developmental timers. In this context, feedback loops among NHR-23/ RORα,
483 LIN-42/PER, and *let-7* family microRNAs appear to preserve the capacity of cells and
484 developing animals to switch between bi-stable states at regular intervals. This provides
485 a different and authentic perspective of related gene regulatory networks that
486 complements and extends current models and applies to human health and disease.

487 **ACKNOWLEDGEMENTS**
488 The American Cancer Society (RSG-12-149-01-DDC to ARF), the National Science
489 Foundation (IOS# 1258218 to ARF), and the School of Medicine at UCLA supported
490 this research. Some strains were provided by the *Caenorhabditis* Genetics Center
491 (CGC), which is funded by the NIH Office of Research Infrastructure Programs (P40
492 OD010440). We thank Amy Pasquinelli (UCSD) and John Kim (Johns Hopkins
493 University) for sharing reagents. We also thank John Kim and Ann Rougvie (University
494 of Minnesota) for helpful discussions and critiques of this manuscript.
495
496 **FIGURE LEGENDS**
497
498 **Figure 1. Longitudinal studies uncover partly interdependent deceleration and**
499 **acceleration of the molting cycle in *nhr-23(RNAi)* and *let-7(n2853)* animals.**
500 **A)** Illustration depicts the phases of the molting cycle reiterated during larval
501 development. **B)** Actograms depict the behavioral states of single animals at regular
502 time samples. Time zero corresponds to the emergence of each larva from the prior
503 molt. Each chart combines records from two independent studies. Criteria used to score
504 animals as active (blue) or lethargic (yellow) during regular time samples are described
505 in the text. **B′)** As above for time samples encompassing L3 and part or all of the L4
506 stage. The strains analyzed were N2, QK059 and MT7626 (not depicted). When
507 cultivated with food for 42 h, 79% of MT7626 larvae and 71% of QK059 larvae
508 developed into young adults, as compared with 12% of N2 worms.
509
510 **Figure 2. The promoter of *let-7* is trans-activated by NHR-23 during late larval**
511 **stages. A)** Schematic of the *let-7* locus shows the correspondence between the
512 minimal promoter (MP), the cluster of ROREs, and the region occupied by NHR-23 in
513 mid-stage larvae. Gray shading demarcates upstream regulatory sequences; black,
514 transcribed sequences; and red, mature *let-7.* The major transcriptional start site (TSS)
515 for pri-*let-7* is labelled. Coordinates refer to *Ce.* Chr. X, as archived in WormBase v.253.
516 **B-C)** Representative fluorescence and DIC images of the lateral epidermis show
517 nuclear-localized GFP driven from the promoter of *let-7*. Arrows point to hyp7 nuclei;
518 arrowheads, seam nuclei. Asterisks mark dividing seam cells. Scale bars = 20 μm.
519 Adjacent scatter plots show aggregated values from two independent trials. Bars signify

520 the mean and sd. ****p≤0.0001, **p≤0.01, Ordinary One-Way ANOVA with Bonferroni's
521 correction for multiple comparisons. **D)** Levels of pri-*let-7* determined by TaqMan
522 qRT-PCR. Each value was normalized to *ama-1* transcript levels in the same sample.
523 All values were then normalized to the mean of all 9 mock-treated time samples.
524 Symbols represent the mean and range from two biological replicates. The x-axis
525 indicates time elapsed (h) on food. The underlying bar depicts developmental stages;
526 gray boxes therein signify observed intervals of behavioral quiescence. The times of
527 initial exposure to *nhr-23* siRNAs and the appearance of molting-defective *nhr-23(RNAi)*
528 larvae are indicated. **E)** As above for levels of mature *let-7*, except that each value was
529 first normalized to U18 levels in the same time sample.
530
531 **Figure 3. Detection of a functional LCS in the 3′UTR of *nhr-23*. A)** Predicted pairing
532 between the transcribed LCS and mature *let-7.* Schematic shows the LCS and similar
533 sites in the *nhr-23* 3′UTR*,* numbered by nt. from the stop codon (black). **B)** Design of
534 bicistronic reporters for 3′UTR-mediated gene regulation. **C)** Representative
535 fluorescence images show tdTomato and GFP co-expressed from bicistronic reporters
536 with the indicated test 3′UTR. The images in each row show the lateral epidermis of one
537 transgenic worm. Arrowheads point to hyp7 nuclei. Scale bar = 10 µm. **D)** Quantitation
538 of related tdTomato/GFP signals observed in two independent experiments. Circles
539 represent the average values from 3 ROIs per worm. Bars signify the mean and sd. N
540 indicates the cumulative sample size. ****p≤0.0001, ***p≤0.001, Ordinary One-Way
541 ANOVA with Tukey's correction for multiple comparisons. **E)** As above, except that
542 ratiometric values were normalized to same-day controls. The full-length *nhr-23*
543 construct is depicted in blue, the deletion constructs in brown.
544
545 **Figure 4. *let-7* down-regulates *nhr-23* while both NHR-23 and *let-7* regulate many**
546 **cyclically-expressed genes. A)** Oscillating *nhr-23* transcript levels detected by
547 TaqMan qRT-PCR in 2 h time samples of *let-7(n28530)* and wild-type animals passing
548 progressing from L2 to adulthood. Boxes beneath the x-axis – shaded as per the legend
549 – signify lethargic intervals. Values were first normalized to *ama-1* transcripts, which
550 encode RNA polymerase II, within each sample. Values were then normalized to the
551 average of all 14 wild-type time samples. **A′)** As above, with time samples of
552 *nhr-23(aaa20)* animals. Cultures were synchronized by passage through L1 diapause.

553 Samples of *let-7(n2853)* and *nhr-23(aaa20)* were collected 22-48 h on food; wild-type,
554 24-50 h on food. Error bars (wild-type values) indicate the range from two qPCR
555 reactions run alongside *let-7(n2853)* and *nhr-23(aaa20)* samples. Supplemental Figure
556 3 shows data from an independent trial. **B)** Quantitation of *mlt-10* transcript levels in the
557 same samples, by the same methods. **C)** Classification of 70 molting-related genes as
558 targets of NHR-23, *let-7s*, both or neither – based on meta-analyses of published data,
559 bioinformatic searches, and systematic rubrics further described in Supplemental Table
560 3. **D-F)** Schematics depict three distinct but related findings that together formulate a
561 cohesive model of the molting timer (see Discussion) **D)** Genetic interactions among
562 *nhr-23*, *let-7s*, and *lin-42* constitute interconnected positive and negative feedback loops
563 – the essential wiring of biological clocks. **E)** Overlapping waves of expression of *nhr-23*
564 and *let-7*. Theoretical curves based on data already described and quantitative imaging
565 of an NHR-23::GFP fusion protein (OP43). RNA and proteins levels are expressed as
566 percentages of peak values; time, as fractions of developmental stages. **F)** Proposed
567 correspondence between levels of NHR-23 and *let-7s*, the expression of critical CCGs,
568 and recurrent transitions between active and quiescent states during larval
569 development.

570 ## STAR METHODS

571 Detailed methods are provided in the online version of this paper and include the
572 following:
573
574 - KEY RESOURCES TABLE
575 - CONTACT FOR REAGENT AND RESOURCE SHARING
576 - EXPERIMENTAL MODEL AND SUBJECT DETAILS
577 - METHOD DETAILS
578 - Working with *C. elegans*
579 - RNA-interference (RNAi)
580 - Longitudinal Studies of the Molting Cycle
581 - Construction of Fusion Genes and Transgenic Strains
582 - Editing the *C. elegans* Genome
583 - Quantitative Fluorescence Microscopy
584 - Isolation of RNA
585 - Quantitative RT-PCR
586 - Bioinformatic Analyses
587 - QUANTIFICATION AND STATISTICAL ANALYSIS
588
589 ## SUPPLEMENTAL INFORMATION

590 The supplemental information for this article includes four figures and two tables.

591 **SUPPLEMENTAL INFORMATION**

592

593 **KEY RESOURCES TABLE**

594

595 **CONTACT FOR REAGENT AND RESOURCE SHARING**

596 Further information and requests for resources and reagents should be directed to and
597 will be fulfilled by the Lead Contact, Alison R. Frand (afrand@mednet.ucla.edu).

598

599 **EXPERIMENTAL MODEL AND SUBJECT DETAILS**

600 Unique strains of the model nematode *Caenorhabditis elegans* generated by and
601 used in this research are described in the Key Resources Table.

602

603 **METHOD DETAILS**

604 **Working with *C. elegans***

605 *C. elegans* were cultivated, observed, transformed and preserved using standard
606 methods (Stiernagle, 2006). Newly-hatched worms were developmentally synchronized
607 by passage through starvation-induced, L1-stage diapause. Hatchlings were isolated by
608 lysis of gravid hermaphrodites in sodium hypochlorite, suspension of eggs in M9 buffer
609 supplemented with 5 μg/mL cholesterol, and incubation for 16 to 24 h with rotational
610 aeration. Hatchlings were released from diapause by plating on solid nematode growth
611 medium (NGM) seeded with *E. coli* OP50-1. One to two hundred larvae were routinely
612 plated on 6 cm NGM plates. Alternatively, ten to fifteen thousand larvae were plated on
613 10 cm NGM plates seeded with 10X concentrated *E. coli* HT115(DE3), as described
614 below. *C. elegans* were cultivated at 25°C unless otherwise specified.

615

616 **RNA-interference (RNAi)**

617 Two clones of *E. coli* HT115(DE3) were used for bacterial-mediated RNAi: one
618 transformed with pPD129.36 (a gift from Andy Fire); the other, with a derivative of
619 pPD129.36 containing *nhr-23* coding sequences. The latter clone was obtained directly
620 from the Ahringer library but matches I-3F11 (Source BioScience). Both clones were
621 cultured and fed to *C. elegans* as described (Kamath et al., 2003), except that NGM
622 was supplemented with 8 mM isopropyl β-D-1-thiogalactopyranoside (Laguna
623 Scientific).

624 To delay silencing of *nhr-23*, L1 larvae were mock-treated for empirically-

625 determined intervals, harvested, washed thrice in M9 and then divided into test and
626 control groups. Test subjects were plated on bacterial lawns that expressed *nhr-23*
627 dsRNAs, while control subjects were re-plated on bacterial lawns that expressed short,
628 dsRNAs unlike any annotated gene in *C. elegans.* Assays involving single worms called
629 for shorter intervals of initial mock-treatment than assays involving thousands of worms
630 per sample. The specific intervals of mock-treatment used in longitudinal studies of
631 worms developing from late L1 to early L3, late L2 to early L4, and late L3 to adulthood
632 were 0, 6, and 14 h, respectively. The intervals of mock-treatment used in studies of
633 gene expression across the same stages were 0, 16, and 24 h. Under the latter
634 conditions peak levels of *nhr-23* transcripts determined by TaqMan qRT-PCR were
635 6.5- and 4.1-times lower in *nhr-23(RNAi)* than wild-type animals harvested during L3
636 and L4, respectively.
637
638 **Longitudinal Studies of the Molting Cycle**
639 Lethargic larvae were isolated from synchronized populations, transferred to
640 individual wells of 12-well NGM plates seeded with *E. coli* HT115(DE3), and observed
641 for 15 s on the hour using a Zeiss M^2BioDiscovery microscope. L3 and younger worms
642 were both observed and videotaped at 600-fold magnification; L4 and older worms, at
643 300-fold magnification. As described, each worm was classified as active or lethargic
644 during each time sample based on defined target behaviors. Molting-defective and
645 ruptured animals were also identified using standard criteria. Worms were videotaped
646 using a Sony HDR-XR500V or Nikon D500 camera attached to the microscope. To
647 measure the pumping rate (Hz) of each specimen, the corresponding film was played
648 back 4-times slower in iMovie version 10.11.2. The number of recorded pharyngeal
649 contractions (pumps) was divided by the duration of the film. Three independent
650 assessments of selected films produced values within 95% of the mean, validating this
651 approach. In Figure 1B, wild-type adults pumped at 3.9 ± 1.1 Hz (mean ± sd). Dark,
652 medium, and light blue signify pumping rates ≥2.8 Hz, 1.7–2.8 Hz, and <1.7 Hz,
653 respectively. In Figure 1B', wild-type animals in the L4 stage pumped at 4.0 ± 1.3 Hz
654 (mean ± sd). Dark, medium, and light blue signify pumping rates ≥2.7 Hz, 1.4–2.7 Hz,
655 and <1.4 Hz, respectively.

656 **Construction of Fusion Genes and Transgenic Strains**

657 The sequences of oligonucleotides used in this study are provided in the Key
658 Resources Table. The bicistronic reporters used to detect regulatory elements within
659 3′UTRs were constructed by Gibson Assembly (NEB) and standard methods. Phusion
660 High-Fidelity DNA Polymerase (NEB) was used to amplify DNA molecules. The
661 resulting plasmids contained the pBR322 backbone of Fire Lab vectors; the *dpy-7*
662 promoter, which corresponds to nucleotides 7,537,914-7,538,219 of *C. elegans* Chr. X
663 (NC_003284); the synthetic intron embedded in primer HM01; the coding sequence for
664 *tandem (td) tomato*, which was isolated from Addgene plasmid #30530 (a gift from
665 Gerhart Ryffel); one of the test 3′UTRs described below; and an *SL2::gfp::unc-54* 3′UTR
666 cassette (a gift from John Kim. The gene-specific 3′UTRs comprised nucleotides
667 amplified from Chr. I (NC_003279) as follows: *nhr-23*, 7,220,953-7,221,820; *unc-54*,
668 14,855,909-14,856,180; and *lin-41*, 9,334,850-9,335,964. Deletions within the *nhr-23*
669 3′UTR reporter (cloned in pHR017) were created using a Q5 Site-Directed Mutagenesis
670 Kit (NEB) and verified by Sanger Sequencing (Genewiz Inc.). To generate distinct
671 extrachromosomal arrays harboring each bicistronic reporter, mixtures of the
672 corresponding plasmid (1ng/µl), the co-transformation marker *ttx-3::gfp* (40ng/µl), and
673 filler DNA pRS316 (59ng/µl) were microinjected into the gonads of wild-type
674 hermaphrodites. Transgenic progeny and unique descendent strains were isolated by
675 standard methods.

676

677 **Editing the *C. elegans* Genome**

678 The CRISPR/Cas9 system was used essentially as described (Paix et al., 2015)
679 to delete the endogenous LCS from the 3′UTR of *nhr-23*, generating the allele
680 *nhr-23(aaa20)*. Briefly, wild-type hermaphrodites were microinjected with a mixture
681 containing the following: *nhr-23* crRNA (400ng/µL), tracrRNA (1µg/µL), *dpy-10* crRNA
682 (160ng/µL, GE Dharmacon), *dpy-10* ssODN (13.75ng/µL, IDT), and CAS9 protein
683 (500ng/µL, PNA Bio) in HEPES buffer pH 7.5 (Sigma-Aldrich) supplemented with
684 0.025µM KCL (Sigma-Aldrich). Injected hermaphrodites (P0s) were singled and
685 screened for Dumpy (Dpy) or Roller (Rol) offspring (F1s), both phenotypes associated
686 with mutations in *dpy-10*. One hundred F1s were singled from a selected P0.
687 Genotyping the F1s and their descendants (F2s) identified two strains homozygous for
688 identical chromosomal deletions of precisely the 21 nucleotides comprising the LCS.

689 One *nhr-23(aaa20)* strain was backcrossed to N2 thrice prior to phenotypic analysis. No
690 edits in the *dpy-10* gene were found in the backcrossed strain (ARF414).
691
692 **Quantitative Fluorescence Microscopy**
693 *C. elegans* were anesthetized with 2.5% NaN_3 (v/v) in M9 buffer, mounted on 2%
694 agarose pads, and observed using a Zeiss Axioplan compound microscope with an
695 attached Hamamatsu Orca ER CCD camera. The image acquisition and analysis
696 software package Volocity 6.3 (Perkin Elmer) was used to control the microscope and
697 digital camera and also to measure average fluorescence intensities within selected
698 regions of interest (ROIs). In particular experiments, transgenic animals were staged
699 partly by DIC microscopy and imaged during the L3/L4 or L4/A molts. Molting animals
700 were identified by occlusion of the buccal cavity (Monsalve et al., 2011). Stereotypical
701 rearrangements of vulva precursor cells (VPCs) demarcated early versus late sub-
702 stages of the L3/L4 molt. The presence of a lumen in the incipient vulva demarcated
703 early versus late sub-stages of the L4/A molt (Gupta et al., 2012; Van Buskirk and
704 Sternberg, 2007).
705 To measure GFP signals associated with the *let-7p::nls-gfp* transcriptional reporter
706 (Kai et al., 2013), worms were imaged at 400X total magnification. Both DIC and
707 fluorescence images of the lateral epidermis were acquired – the latter with an exposure
708 time of 25ms. Three nuclei in hyp7 and three in the seam were traced from the DIC
709 image of each worm. The average fluorescence intensity within each nucleus was then
710 measured and corrected for background signal. The average values for both hyp7 and
711 seam nuclei (per worm) were used in further statistical analysis.
712 Signals associated with tdTomato and GFP expressed from bicistronic reporters
713 for regulatory elements within 3′UTRs were measured using similar approaches. In this
714 case, three distinct ROIs with areas of 40–70um^2 were manually selected per worm;
715 each ROI included approximately equal areas of the nucleus and cytoplasm. In addition,
716 multiple images of tdTomato and GFP were automatically captured over a range of
717 exposure times. The average fluorescence intensity of each ROI was measured and
718 plotted versus the exposure time. Values within the linear range of the assay were then
719 used to determine the ratiometric signal (tdTomato/GFP) for each ROI. The average
720 ratiometric value of all three ROIs per worm was used for subsequent statistical
721 analysis. Notably, the morphology of the vulva was abnormal in a subset (≤ 10%) of

722 animals that expressed any bicistronic reporter. Because the phenotype precluded
723 staging by the abovementioned criteria, this subset of animals was excluded from the
724 analysis.
725
726 **Isolation of RNA**
727 RNA was extracted from developmentally synchronized *C. elegans* as described
728 (McCulloch and Rougvie, 2014). Using light microscopy, the fraction of pumping (active)
729 versus non-pumping (lethargic) animals in each sample was counted prior to collection
730 (n = 50-100). Troughs in the percentage of pumping animals were used to delimit
731 quiescent intervals *post-hoc.* Pellets containing ten to fifteen thousand worms (~100 µl)
732 were re-suspended in 4 volumes of TRIzol (ThermoFisher Scientific) and 1 volume of
733 glass beads 400-625 µm in diameter (Sigma). The suspensions were vortexed, flash
734 frozen, and thawed thrice. Samples were then mixed with 0.17 volumes of 24:1
735 chloroform: isoamyl alcohol (OmniPur) and centrifuged. The aqueous layer was
736 collected, mixed with an equal volume of 5:1 acid phenol: chloroform (ThermoFisher
737 Scientific), and centrifuged again. After collection of the top layer, RNA was extracted by
738 precipitation with ice-cold isopropanol (Sigma) and GlycoBlue (ThermoFisher Scientific).
739 The concentration of RNA in each time sample was measured using a NanoDrop 2000
740 (ThermoFisher Scientific). Thereafter, 5 µg of total RNA per sample was treated with 2U
741 of TURBO DNase (ThermoFisher Scientific) for 1 h. Notably, RNA samples used to
742 quantify mature *let-7* were not pre-treated with DNAse.
743
744 **Quantitative RT-PCR**
745 The sequences of gene-specific RT primers and identifiers for TaqMan assays
746 used in this research are provided in the Key Resources Table. To quantify levels of
747 primary *let-7* and *ama-1* transcripts in the abovementioned extracts, we processed 50ng
748 of RNA using a High-Capacity cDNA Reverse Transcription Kit (ThermoFisher
749 Scientific). Reaction mixtures of 15µL included random primers, dNTPs, RNaseOUT,
750 and reverse transcriptase, per the manufacturer's guidelines. To quantify levels of
751 mature *let-7* and the U18 small nucleolar (sno) RNA, we processed RNA with the same
752 kit but used gene-specific rather than random primers. Three volumes of nuclease-free
753 water were added to completed RT reactions. Next, we set-up TaqMan assays
754 (ThermoFisher Scientific) in 96-well plates, in triplicate. Per the manufacturer's

755 instructions, each reaction included TaqMan Universal PCR Master Mix, no AmpErase
756 UNG, gene-specific primers, and 1.3μL of the preceding RT product in a volume of
757 20μL. Reactions ran on a Stratagene MX3000P (Agilent Genomics). To measure levels
758 of protein-coding transcripts, 1μg of RNA was reverse transcribed using the enzyme
759 Transcriptor (Roche). Each reaction mixture (20μL) also included hexadeoxynucleotide
760 primers (Promega), dNTPs and RNasin (Promega). Four volumes of nuclease-free
761 water were added to completed RT reactions. TaqMan assays were performed as
762 described using 2μL of the RT product as template in a volume of 10μL.
763 The amount of template used in each TaqMan assay gave Ct values in the linear
764 range of 21 to 36. In nearly all cases, technical replicates gave Ct values within 95% of
765 the mean and the mean Ct value was used in subsequent analyses. Separate TaqMan
766 reactions using templates made in the absence of reverse transcriptase produced no
767 detectable PCR products, confirming the amplification of RNA rather than genomic
768 DNA. As described, the levels of transcripts of interest were normalized to the levels of
769 *ama-1* mRNAs or U18 snoRNAs within each sample, which were quantified in parallel
770 TaqMan assays. For studies of gene expression over several developmental stages, the
771 normalized values for each time sample were further standardized to the mean of all
772 time samples derived from mock-treated or wild-type animals.
773
774 **Bioinformatic Analyses**
775 DNA sequences corresponding to the upstream regulatory region, first intron and
776 3′UTR for each nematode gene of interest were retrieved from WormBase (WS) v.264
777 and saved as SnapGene v.4 (GSL Biotech) files. The upstream sequences extracted
778 from WS included all nucleotides between the transcriptional start site of the gene of
779 interest and the nearest protein-coding gene. Particular sequences were extended or
780 shortened based on gene models, ESTs and transcriptional start sites archived in
781 WS264. If the gene of interest lacked an annotated 3′UTR, then we initially retrieved 1
782 kb of sequence downstream of the stop codon. Particular 3′UTR sequences were
783 revised based on ESTs and poly-AAA sites that are archived in WS264 but not yet
784 incorporated in current gene models.
785 Both the upstream regulatory regions of vertebrate homologs of *let-7* and the
786 3′UTRs of vertebrate homologs of *nhr-23*/*RORs* were retrieved from the UCSC genome
787 browser. Three human genes, two mouse genes, and six zebrafish genes encode

788 mature miRNAs identical in sequence to *C. elegans let-7*. We extracted 3 kb of
789 sequence upstream of each *let-7* homolog, except in the case of *H. sapiens let-7a-3*,
790 wherein the core promoter has been experimentally delimited to 1 kb of upstream
791 sequence (Wang et al., 2012). For a given gene, the longest 3′UTR was selected if
792 multiple 3′UTRs existed. The 3′UTR sequences were individually and systematically
793 validated by comparison with EST; only those genes with annotated 3′UTRs supported
794 by ESTs were included in further analyses.

795 To identify ROR response elements that might function as transcriptional
796 enhancers of miRNAs or protein-coding genes of interest, we searched the upstream
797 regulatory sequences and/or first introns for instances of the consensus response
798 element 5′-(A/G)GGTCA-3′ on both the coding and anti-coding strands of DNA. Figure
799 1A and Supplemental Figures 1A and 4A depict the results of these computational
800 searches. To accurately calculate the probability of an RORE occurring by chance, we
801 first used the k-mer counting software program DSK (Rizk G. et al, 2013) to determine
802 that the reference genome of *C. elegans*, which comprises 100.2 mega bases, includes
803 41,203 distinct instances of the consensus RORE. For non-nematodes, the expected
804 frequency was the chance of either six-nucleotide sequence appearing in a longer
805 oligonucleotide; this frequency is approximately one per 1 kb.

806 Regions of *C. elegans* chromosomal DNA occupied by NHR-23 *in vivo* were
807 identified on the modEncode *C. elegans* Genome Browser (v. 2.48). The two relevant
808 datasets archived therein were Chip-Seq of strain OP43 cultivated at 20°C and
809 harvested during the L2 or L3 stage. Most ID in L3, addition in L2. Both used – not
810 discriminate the two here. The upstream regulatory sequences and/or first intron for
811 each gene of interest were viewed in this browser. Regions of significant enrichment
812 ("peaks") were identified by z-scores ≥ 2 (Celniker et al., 2009). Sequences extracted
813 and aligned with the upstream regulatory regions and/or first intron as above, adjusting
814 for differences in the related chromosomal coordinates between WS220 and WS264.

815 Evidence of direct or indirect regulation of transcript levels by NHR-23 was either
816 detected by Affymetrix microarrays in 2-3/3 biological replicates (Kouns et al., 2011), or
817 shown prior publications (*lin-42a/b*, *nas-36*). Expression was at least 1.2-fold lower in
818 *nhr-23* knockdowns than mock-treated larvae.

819 Targets of NHR-23 followed 2 out of the 3 following criteria: 1) The upstream
820 regulatory region and/or first intron contained Chip-Seq NHR-23 peaks (Celniker et al.,

821 2009); 2) the same region contained more ROREs than predicted by chance alone; and
822 3) Expression was 1.2-fold lower in *nhr-23* knockdowns than mock-treated larvae.
823 The software RNAhybrid (Rehmsmeier et al., 2004) was used to detect
824 sequences partially complementary to the 21-nt. mature *let-7* in the 3′UTRs of
825 annotated homologs of *nhr-23* in the genomes of *H. sapiens*, *M. musculus*, *D. rerio* and
826 *C. briggsae*. Mature *C. elegans let-7*, which is identical to human *let-7*a, was used as
827 the query sequence. No more than 1 mismatched nucleotide within the *let-7* seed
828 sequence was tolerated for the prediction of LCSs in this report.
829 Targets of *let-7* fulfilled both of the following criteria: 1) LCSs, with up to one
830 mismatch in the seed region, were detected in the 3′UTR more often than, or equal to,
831 the number predicted by chance alone (Rehmsmeier et al., 2004); and (2) ALG-1 co-IP
832 the 3′UTR, on the coding strand of the gene by iCLIP-Seq (Broughton et al., 2016).
833 Genes were determined to be “involved in molting” based on the literature. For
834 example, if mutations in a particular gene caused a molting defective phenotype, the
835 gene was considered to be involved in molting (Frand et al., 2005). Similarly, if
836 inactivation of the gene had an effect on lethargus, the gene was also considered to be
837 involved in the molting cycle.
838 Genes were annotated as “oscillatory” based on published RNA-Seq studies
839 (Hendriks et al., 2014; Kim et al., 2013); therein, genes whose expression at 8-10 h
840 intervals was significantly correlated ($P<0.05$) were considered to be cycling in
841 expression.
842
843 **QUANTIFICATION AND STATISTICAL ANALYSIS**
844 The software package Volocity 6.3 (Perkin Elmer) was used to BOTH acquire
845 fluorescence micrographs and measure the signal intensity of selected ROIs. The
846 software package GraphPad Prism v6.0h was used for all statistical tests. Samples
847 sizes for all experiments, statistical analysis, and outcomes thereof are specified in each
848 figure and/or corresponding legend.

849 **SUPPLEMENTAL FIGURE LEGENDS**

850

851 **Supplemental Figure 1. NHR-23 activates pulsatile expression of the *lin-42* gene**.
852 **A)** Schematic shows the correspondence among annotated regulatory regions of seven
853 *lin-42* variants (WS264) and ten chromosomal regions occupied by NHR-23 in mid-
854 stage larvae. Dashed lines demarcate defined promoters; arrows label transcriptional
855 start sites. Coordinates refer to *C. elegans* Chr. II (NC_003280). **B)** Relative levels of
856 *lin-42* transcripts detected in *nhr-23(RNAi)* versus mock-treated animals by TaqMan
857 qRT-PCR. Each value was first normalized to *ama-1* transcript levels in the same
858 sample. All values were then normalized to the mean of all mock-treated time samples.
859 Symbols represent the mean and range from two biological replicates. The x-axis
860 indicates time elapsed (h) on food. Bars beneath the x-axis depict progression of the life
861 cycle; gray boxes therein signify observed intervals of quiescence. The times of initial
862 exposure to *nhr-23* siRNAs and the appearance of molting-defective *nhr-23(RNAi)*
863 larvae are indicated.

864

865 **Supplemental Figure 2. Proposed molecular mechanism for the bicistronic**
866 **reporter system.** Schematic depicts expression from the *dpy-7* promoter and trans-
867 splicing followed by standalone translation of tdTomato and GFP. (Left) Equimolar
868 levels of tdTomato and GFP in the absence of 3′UTR-mediated repression. To predict
869 the resulting ratiometric signal, the synthesis and degradation of transcripts and proteins
870 were considered equally efficient. If so, then a ratiometric signal of 2.4 was expected,
871 based on the brightness of tdTomato and GFP, respectively, 95 and 39 $(mM•cm)^{-1}$
872 (Shaner et al., 2005). (Right) Anticipated events for a 3'UTR targeted by a miRNA. The
873 illustration depicts *let-7*, specifically, because the test 3'UTRs all contained
874 complementary sites. concept

875

876 **Supplemental Figure 3. The LCS mediates repression of *nhr-23* from late L2**
877 **through young adulthood. A-A′)** Normalized levels of *nhr-23* transcripts detected by
878 TaqMan qRT-PCR in regular 2 h time samples of *let-7(n2853)*, *nhr-23(aaa20)* and wild-
879 type animals. Values obtained from an independent trial are presented as per Figure
880 4A. Note that these time samples include a relatively small fraction of the adult stage.
881 All three samples were collected after 24-50 h on food. **B)** As above, for *nhr-23*

882 transcripts detected in *mir-41(Δ) mir-241(Δ); mir-84(n4037)* triple mutants,
883 *nhr-23(aaa20)* single mutants, and wild-type larvae progressing from late L1 through
884 mid L3. Both the *let-7s* triple knockout and wild-type larvae were collected 14–26 h after
885 release from starvation; *nhr-23(aaa20)* larvae, 16–28 h after release.
886
887 **Supplemental Figure 4. Reciprocal target sequences for RORs and *let*-7-family**
888 **miRNAs identified in vertebrates. A)** Schematics show ROREs (brown), upstream
889 regulatory sequences (gray), and homologs of mature *let-7* (pink) found in annotated
890 genomes of the indicated species. Arrows are aesthetic landmarks for as-yet undefined
891 transcriptional start sites. B) Schematics show LCSs (gold), 3′UTRs (blue), and stop
892 codons (black) of annotated *ROR* homologs. Gradients and bold labels distinguish sites
893 perfectly complementary to the seed of *let-7s*. The selected 3′UTRs were retrieved from
894 the UCSC genome browser; verified by curated ESTs; and searched using RNAhybrid.
895 Supplemental Table 2 includes more information about the depicted LCSs.
896
897 **Supplemental Table 1. Comparative Metrics of Molting Biorhythms.**
898 Chart includes the average duration (h) of active and lethargic intervals, and also the
899 wake-to-wake interval, for cohorts of *nhr-23(RNAi)*, *let-7*-family mutants and wild-type
900 animals progressing through the indicated stages. ****$p<0.0001$, ***$p\leq0.001$, *$p\leq0.05$ for
901 pairwise comparisons with age-matched, mock-treated wild-type cohorts; Ordinary One-
902 Way ANOVA with Bonferroni's correction for multiple comparisons. All animals were
903 cultivated on *E. coli* HT115(DE3) transformed by empty vector unless otherwise
904 specified.
905
906 **Supplemental Table 2. LCSs found in nematode and vertebrate homologs of *ROR*.**
907 Entries correspond to sites shown in Supplemental Figure 4B. The number of nt.
908 between the 3′ end of each LCS and the stop codon is specified. Thermostability values
909 for RNA duplexes between mature *let-7* and each LCS were predicted using
910 RNAhybrid**.** The predicted values for all entries are lower than predicted thermostability
911 of duplexes between *let-7* and its target site in the 3′UTR of *lin-41,* which is -29 kcal/mol
912 (Rehmsmeier et al., 2004)
913

914 **Supplemental Table 3. Classification of genes linked to molting as targets of**
915 **NHR-23, *let*-7s, neither or both.** The bioinformatic approaches and criteria for
916 assignment of queries to categories are described in the detailed methods. The name
917 and WormBase accession number of each gene is listed. The value of "# Obs/# Exp" in
918 column 5 indicates the ratio of the number of ROREs observed to the number expected
919 by chance alone, as described in the Methods. Genes that were detected as down
920 regulated in *nhr-23(RNAi)* animals, relative to controls, using microarray analysis or
921 other techniques, are indicated as "↓" in column 6. A "Y" in column 7 indicates that the
922 gene was considered a target of NHR-23. The value of "# Obs/# Exp" in column 11
923 indicates the ratio of the number of LCSs observed to the number expected by chance
924 alone, as described in the Methods. Genes with 3′UTRs bound by ALG-1 are indicated
925 by a "+" symbol in column 12. A "Y" in column 13 indicates that a particular gene was
926 considered a target of let-7. A "≈" in column 15 indicates that expression of the gene
927 oscillates throughout development.

928 **REFERENCES**

929 Abbott, A.L., Alvarez-Saavedra, E., Miska, E.A., Lau, N.C., Bartel, D.P., Horvitz, H.R.,
930 and Ambros, V. (2005). The let-7 MicroRNA family members mir-48, mir-84, and mir-
931 241 function together to regulate developmental timing in Caenorhabditis elegans. Dev
932 Cell *9*, 403-414.
933 Ambros, V., and Ruvkun, G. (2018). Recent Molecular Genetic Explorations of
934 Caenorhabditis elegans MicroRNAs. Genetics *209*, 651-673.
935 Antebi, A. (2015). Nuclear receptor signal transduction in C. elegans. WormBook, 1-49.
936 Bethke, A., Fielenbach, N., Wang, Z., Mangelsdorf, D.J., and Antebi, A. (2009). Nuclear
937 hormone receptor regulation of microRNAs controls developmental progression.
938 Science *324*, 95-98.
939 Bracht, J., Hunter, S., Eachus, R., Weeks, P., and Pasquinelli, A.E. (2004). Trans-
940 splicing and polyadenylation of let-7 microRNA primary transcripts. RNA *10*, 1586-1594.
941 Broughton, J.P., Lovci, M.T., Huang, J.L., Yeo, G.W., and Pasquinelli, A.E. (2016).
942 Pairing beyond the Seed Supports MicroRNA Targeting Specificity. Mol Cell *64*, 320-
943 333.
944 Celniker, S.E., Dillon, L.A., Gerstein, M.B., Gunsalus, K.C., Henikoff, S., Karpen, G.H.,
945 Kellis, M., Lai, E.C., Lieb, J.D., MacAlpine, D.M.*, et al.* (2009). Unlocking the secrets of
946 the genome. Nature *459*, 927-930.
947 Chen, D., Taylor, K.P., Hall, Q., and Kaplan, J.M. (2016). The Neuropeptides FLP-2 and
948 PDF-1 Act in Concert To Arouse Caenorhabditis elegans Locomotion. Genetics *204*,
949 1151-1159.
950 Cook, D.N., Kang, H.S., and Jetten, A.M. (2015). Retinoic Acid-Related Orphan
951 Receptors (RORs): Regulatory Functions in Immunity, Development, Circadian Rhythm,
952 and Metabolism. Nucl Receptor Res *2*.
953 Driver, R.J., Lamb, A.L., Wyner, A.J., and Raizen, D.M. (2013). DAF-16/FOXO regulates
954 homeostasis of essential sleep-like behavior during larval transitions in C. elegans. Curr
955 Biol *23*, 501-506.
956 Ecsedi, M., Rausch, M., and Grosshans, H. (2015). The let-7 microRNA directs vulval
957 development through a single target. Dev Cell *32*, 335-344.
958 Edelman, T.L., McCulloch, K.A., Barr, A., Frokjaer-Jensen, C., Jorgensen, E.M., and
959 Rougvie, A.E. (2016). Analysis of a lin-42/Period Null Allele Implicates All Three
960 Isoforms in Regulation of Caenorhabditis elegans Molting and Developmental Timing.
961 G3 (Bethesda).
962 El-Sherif, E., Averof, M., and Brown, S.J. (2012). A segmentation clock operating in
963 blastoderm and germband stages of Tribolium development. Development *139*, 4341-
964 4346.
965 Frand, A.R., Russel, S., and Ruvkun, G. (2005). Functional genomic analysis of C.
966 elegans molting. PLoS Biol *3*, e312.
967 Galles, C., Prez, G.M., Penkov, S., Boland, S., Porta, E.O.J., Altabe, S.G., Labadie,
968 G.R., Schmidt, U., Knolker, H.J., Kurzchalia, T.V.*, et al.* (2018). Endocannabinoids in
969 Caenorhabditis elegans are essential for the mobilization of cholesterol from internal
970 reserves. Sci Rep *8*, 6398.
971 Gomez, C., Ozbudak, E.M., Wunderlich, J., Baumann, D., Lewis, J., and Pourquie, O.
972 (2008). Control of segment number in vertebrate embryos. Nature *454*, 335-339.
973 Gupta, B.P., Hanna-Rose, W., and Sternberg, P.W. (2012). Morphogenesis of the vulva
974 and the vulval-uterine connection. WormBook, 1-20.

975 Hammell, C.M., Karp, X., and Ambros, V. (2009). A feedback circuit involving let-7-
976 family miRNAs and DAF-12 integrates environmental signals and developmental timing
977 in Caenorhabditis elegans. Proc Natl Acad Sci U S A *106*, 18668-18673.
978 Hayes, G.D., Frand, A.R., and Ruvkun, G. (2006). The mir-84 and let-7 paralogous
979 microRNA genes of Caenorhabditis elegans direct the cessation of molting via the
980 conserved nuclear hormone receptors NHR-23 and NHR-25. Development *133*, 4631-
981 4641.
982 Hendriks, G.J., Gaidatzis, D., Aeschimann, F., and Grosshans, H. (2014). Extensive
983 oscillatory gene expression during C. elegans larval development. Mol Cell *53*, 380-392.
984 Isik, M., Blackwell, T.K., and Berezikov, E. (2016). MicroRNA mir-34 provides
985 robustness to environmental stress response via the DAF-16 network in C. elegans. Sci
986 Rep *6*, 36766.
987 Iwanir, S., Tramm, N., Nagy, S., Wright, C., Ish, D., and Biron, D. (2013). The
988 microarchitecture of C. elegans behavior during lethargus: homeostatic bout dynamics,
989 a typical body posture, and regulation by a central neuron. Sleep *36*, 385-395.

990 Jeon, M., Gardner, H.F., Miller, E.A., Deshler, J., and Rougvie, A.E. (1999). Similarity of
991 the C. elegans developmental timing protein LIN-42 to circadian rhythm proteins.
992 Science *286*, 1141-1146.
993 Johnson, S.M., Lin, S.Y., and Slack, F.J. (2003). The time of appearance of the C.
994 elegans let-7 microRNA is transcriptionally controlled utilizing a temporal regulatory
995 element in its promoter. Dev Biol *259*, 364-379.
996 Kai, Z.S., Finnegan, E.F., Huang, S., and Pasquinelli, A.E. (2013). Multiple cis-elements
997 and trans-acting factors regulate dynamic spatio-temporal transcription of let-7 in
998 Caenorhabditis elegans. Dev Biol *374*, 223-233.
999 Kamath, R.S., Fraser, A.G., Dong, Y., Poulin, G., Durbin, R., Gotta, M., Kanapin, A., Le
1000 Bot, N., Moreno, S., Sohrmann, M.*, et al.* (2003). Systematic functional analysis of the
1001 Caenorhabditis elegans genome using RNAi. Nature *421*, 231-237.
1002 Kim, D., Grun, D., and van Oudenaarden, A. (2013). Dampening of expression
1003 oscillations by synchronous regulation of a microRNA and its target. Nat Genet *45*,
1004 1337-1344.
1005 Kostrouchova, M., Krause, M., Kostrouch, Z., and Rall, J.E. (1998). CHR3: a
1006 Caenorhabditis elegans orphan nuclear hormone receptor required for proper epidermal
1007 development and molting. Development *125*, 1617-1626.
1008 Kouns, N.A., Nakielna, J., Behensky, F., Krause, M.W., Kostrouch, Z., and
1009 Kostrouchova, M. (2011). NHR-23 dependent collagen and hedgehog-related genes
1010 required for molting. Biochem Biophys Res Commun *413*, 515-520.
1011 Matsu-Ura, T., Dovzhenok, A., Aihara, E., Rood, J., Le, H., Ren, Y., Rosselot, A.E.,
1012 Zhang, T., Lee, C., Obrietan, K.*, et al.* (2016). Intercellular Coupling of the Cell Cycle
1013 and Circadian Clock in Adult Stem Cell Culture. Mol Cell *64*, 900-912.
1014 McCulloch, K.A., and Rougvie, A.E. (2014). Caenorhabditis elegans period homolog lin-
1015 42 regulates the timing of heterochronic miRNA expression. Proc Natl Acad Sci U S A
1016 *111*, 15450-15455.
1017 Meli, V.S., Osuna, B., Ruvkun, G., and Frand, A.R. (2010). MLT-10 defines a family of
1018 DUF644 and proline-rich repeat proteins involved in the molting cycle of Caenorhabditis
1019 elegans. Mol Biol Cell *21*, 1648-1661.
1020 Monsalve, G.C., Van Buskirk, C., and Frand, A.R. (2011). LIN-42/PERIOD controls
1021 cyclical and developmental progression of C. elegans molts. Curr Biol *21*, 2033-2045.

Nelson, M.D., Lee, K.H., Churgin, M.A., Hill, A.J., Van Buskirk, C., Fang-Yen, C., and Raizen, D.M. (2014). FMRFamide-like FLP-13 neuropeptides promote quiescence following heat stress in Caenorhabditis elegans. Curr Biol *24*, 2406-2410.

Olmedo, M., Merrow, M., and Geibel, M. (2017). Sleeping Beauty? Developmental Timing, Sleep, and the Circadian Clock in Caenorhabditis elegans. Adv Genet *97*, 43-80.

Paix, A., Folkmann, A., Rasoloson, D., and Seydoux, G. (2015). High Efficiency, Homology-Directed Genome Editing in Caenorhabditis elegans Using CRISPR-Cas9 Ribonucleoprotein Complexes. Genetics *201*, 47-54.

Perales, R., King, D.M., Aguirre-Chen, C., and Hammell, C.M. (2014). LIN-42, the Caenorhabditis elegans PERIOD homolog, negatively regulates microRNA transcription. PLoS Genet *10*, e1004486.

Raizen, D.M., Zimmerman, J.E., Maycock, M.H., Ta, U.D., You, Y.J., Sundaram, M.V., and Pack, A.I. (2008). Lethargus is a Caenorhabditis elegans sleep-like state. Nature *451*, 569-572.

Rehmsmeier, M., Steffen, P., Hochsmann, M., and Giegerich, R. (2004). Fast and effective prediction of microRNA/target duplexes. RNA *10*, 1507-1517.

Reinhart, B.J., Slack, F.J., Basson, M., Pasquinelli, A.E., Bettinger, J.C., Rougvie, A.E., Horvitz, H.R., and Ruvkun, G. (2000). The 21-nucleotide let-7 RNA regulates developmental timing in Caenorhabditis elegans. Nature *403*, 901-906.

Santori, F.R., Huang, P., van de Pavert, S.A., Douglass, E.F., Jr., Leaver, D.J., Haubrich, B.A., Keber, R., Lorbek, G., Konijn, T., Rosales, B.N.*, et al.* (2015). Identification of natural RORgamma ligands that regulate the development of lymphoid cells. Cell Metab *21*, 286-298.

Shaner, N.C., Steinbach, P.A., and Tsien, R.Y. (2005). A guide to choosing fluorescent proteins. Nat Methods *2*, 905-909.

Singh, K., Chao, M.Y., Somers, G.A., Komatsu, H., Corkins, M.E., Larkins-Ford, J., Tucey, T., Dionne, H.M., Walsh, M.B., Beaumont, E.K.*, et al.* (2011). C. elegans Notch signaling regulates adult chemosensory response and larval molting quiescence. Curr Biol *21*, 825-834.

Singh, R.N., and Sulston, J.E. (1978). Some observations on moulting in Caenorhabditis elegans. Nematologica *24*, 63-71.

Sparrow, D.B., Chapman, G., Turnpenny, P.D., and Dunwoodie, S.L. (2007). Disruption of the somitic molecular clock causes abnormal vertebral segmentation. Birth Defects Res C Embryo Today *81*, 93-110.

Stiernagle, T. (2006). Maintenance of C. elegans. WormBook, 1-11.

Takahashi, J.S. (2016). Molecular Architecture of the Circadian Clock in Mammals. In A Time for Metabolism and Hormones, P. Sassone-Corsi, and Y. Christen, eds. (Cham (CH)), pp. 13-24.

Takahashi, J.S. (2017). Transcriptional architecture of the mammalian circadian clock. Nat Rev Genet *18*, 164-179.

Timmons, L., Court, D.L., and Fire, A. (2001). Ingestion of bacterially expressed dsRNAs can produce specific and potent genetic interference in Caenorhabditis elegans. Gene *263*, 103-112.

Trojanowski, N.F., and Raizen, D.M. (2016). Call it Worm Sleep. Trends Neurosci *39*, 54-62.

Ueda, H.R., Chen, W., Adachi, A., Wakamatsu, H., Hayashi, S., Takasugi, T., Nagano, M., Nakahama, K., Suzuki, Y., Sugano, S.*, et al.* (2002). A transcription factor response element for gene expression during circadian night. Nature *418*, 534-539.

Van Buskirk, C., and Sternberg, P.W. (2007). Epidermal growth factor signaling induces behavioral quiescence in Caenorhabditis elegans. Nat Neurosci *10*, 1300-1307.

Van Wynsberghe, P.M., Finnegan, E.F., Stark, T., Angelus, E.P., Homan, K.E., Yeo, G.W., and Pasquinelli, A.E. (2014). The Period protein homolog LIN-42 negatively regulates microRNA biogenesis in C. elegans. Dev Biol *390*, 126-135.

Van Wynsberghe, P.M., Kai, Z.S., Massirer, K.B., Burton, V.H., Yeo, G.W., and Pasquinelli, A.E. (2011). LIN-28 co-transcriptionally binds primary let-7 to regulate miRNA maturation in Caenorhabditis elegans. Nat Struct Mol Biol *18*, 302-308.

Vella, M.C., Choi, E.Y., Lin, S.Y., Reinert, K., and Slack, F.J. (2004). The C. elegans microRNA let-7 binds to imperfect let-7 complementary sites from the lin-41 3'UTR. Genes Dev *18*, 132-137.

Wang, D.J., Legesse-Miller, A., Johnson, E.L., and Coller, H.A. (2012). Regulation of the let-7a-3 promoter by NF-kappaB. PLoS One *7*, e31240.

Zhang, Y., Papazyan, R., Damle, M., Fang, B., Jager, J., Feng, D., Peed, L.C., Guan, D., Sun, Z., and Lazar, M.A. (2017). The hepatic circadian clock fine-tunes the lipogenic response to feeding through RORalpha/gamma. Genes Dev.

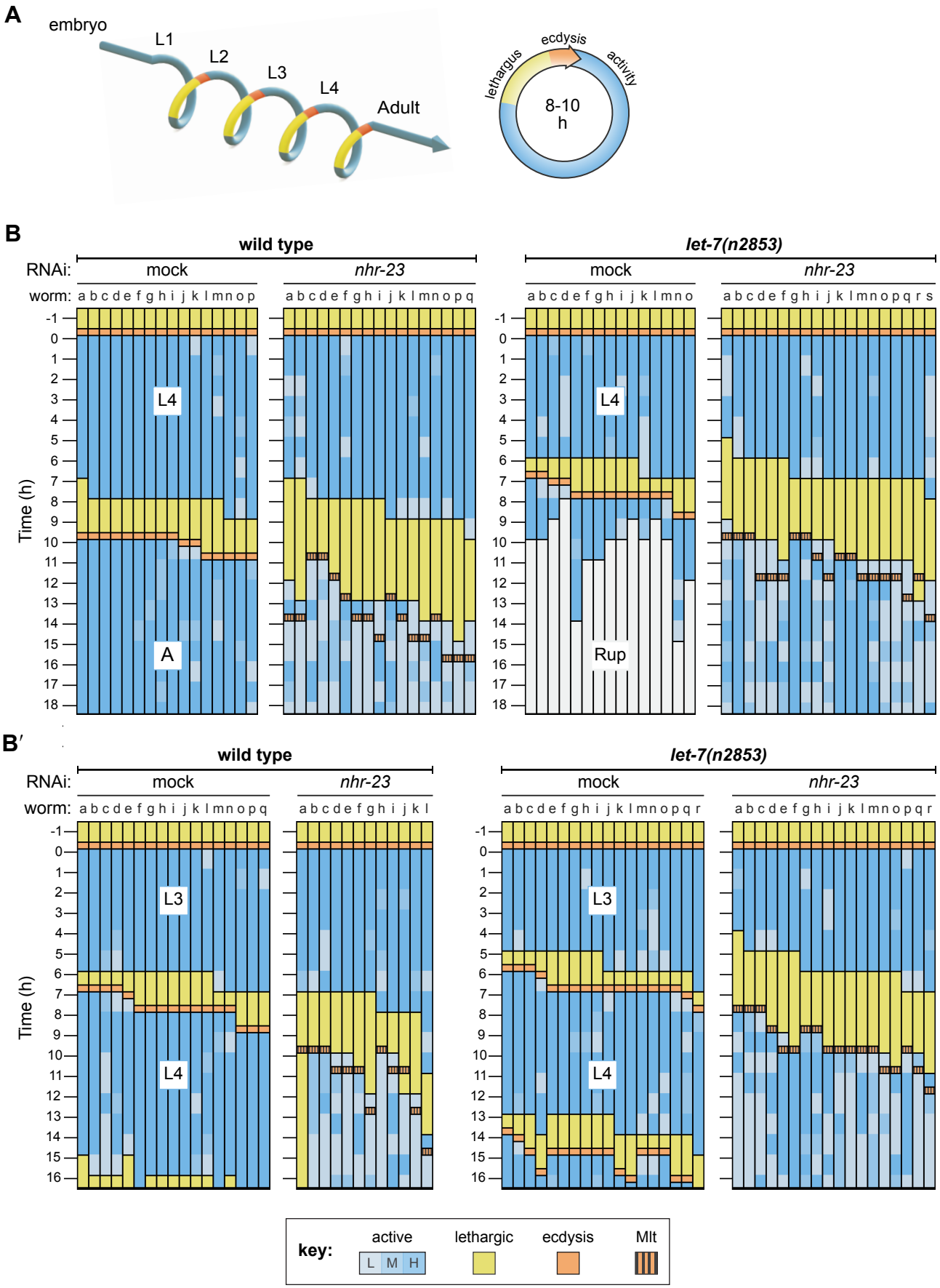
A
embryo
L1
L2
L3
L4
Adult
ecdysis
lethargus
activity
8-10 h
B
wild type
let-7(n2853)
RNAi:
mock
nhr-23
worm:
Time (h)
L4
A
Rup
B′
L3
key:
active
L M H
lethargic
ecdysis
Mlt

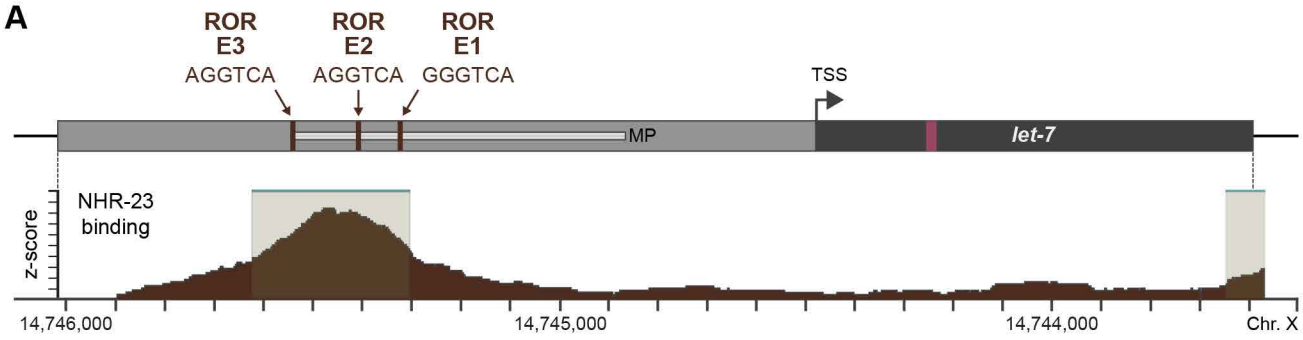
A
ROR E3
AGGTCA
ROR E2
AGGTCA
ROR E1
GGGTCA
TSS
MP
let-7
NHR-23 binding
z-score
14,746,000
14,745,000
14,744,000
Chr. X

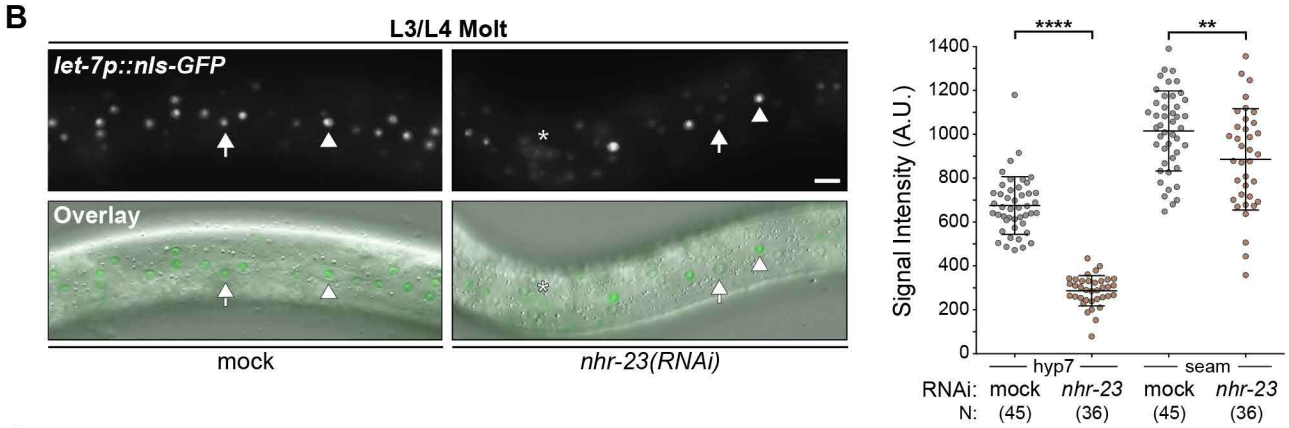
B
L3/L4 Molt
let-7p::nls-GFP
Overlay
mock
nhr-23(RNAi)
Signal Intensity (A.U.)
****
**
hyp7
seam
RNAi: mock nhr-23 mock nhr-23
N: (45) (36) (45) (36)

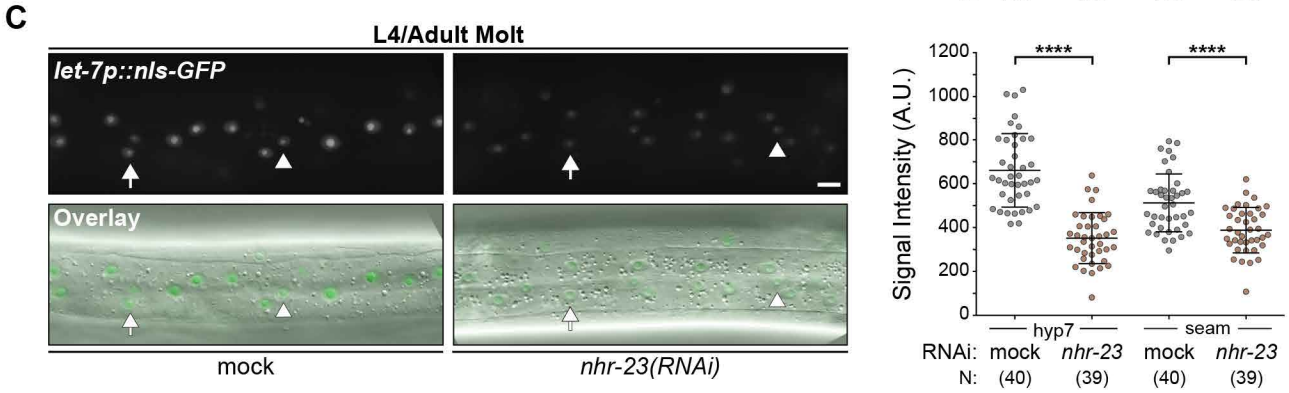
C
L4/Adult Molt
let-7p::nls-GFP
Overlay
mock
nhr-23(RNAi)
Signal Intensity (A.U.)
****
****
hyp7
seam
RNAi: mock nhr-23 mock nhr-23
N: (40) (39) (40) (39)

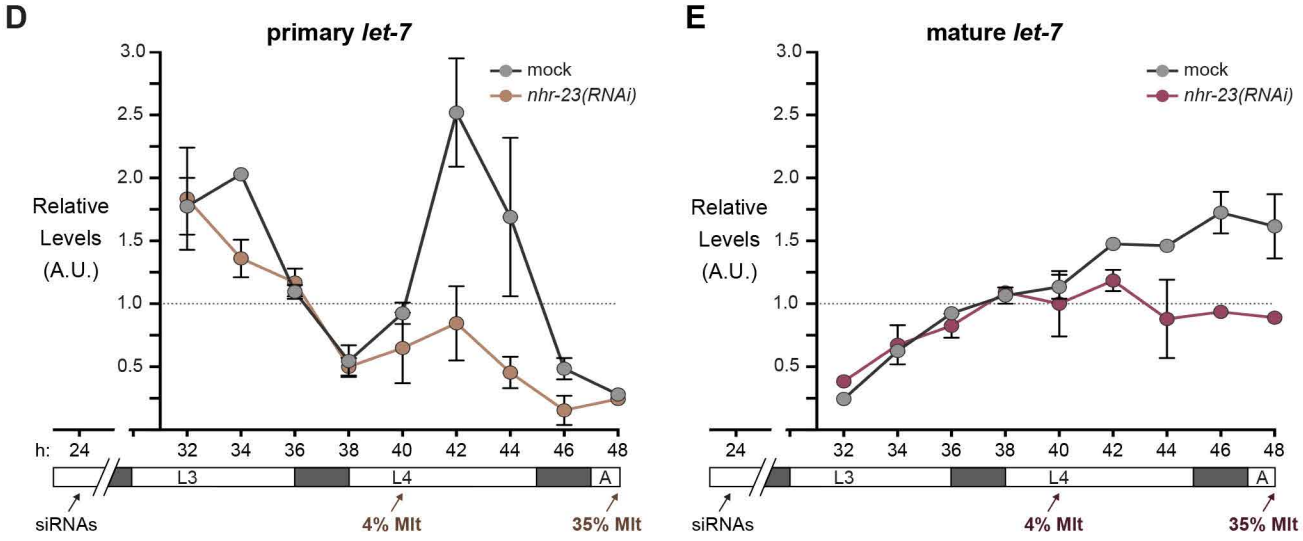
D
primary let-7
mock
nhr-23(RNAi)
Relative Levels (A.U.)
h: 24 32 34 36 38 40 42 44 46 48
L3
L4
A
siRNAs
4% Molt
35% Molt
E
mature let-7
mock
nhr-23(RNAi)
Relative Levels (A.U.)
24 32 34 36 38 40 42 44 46 48
L3
L4
A
siRNAs
4% Molt
35% Molt

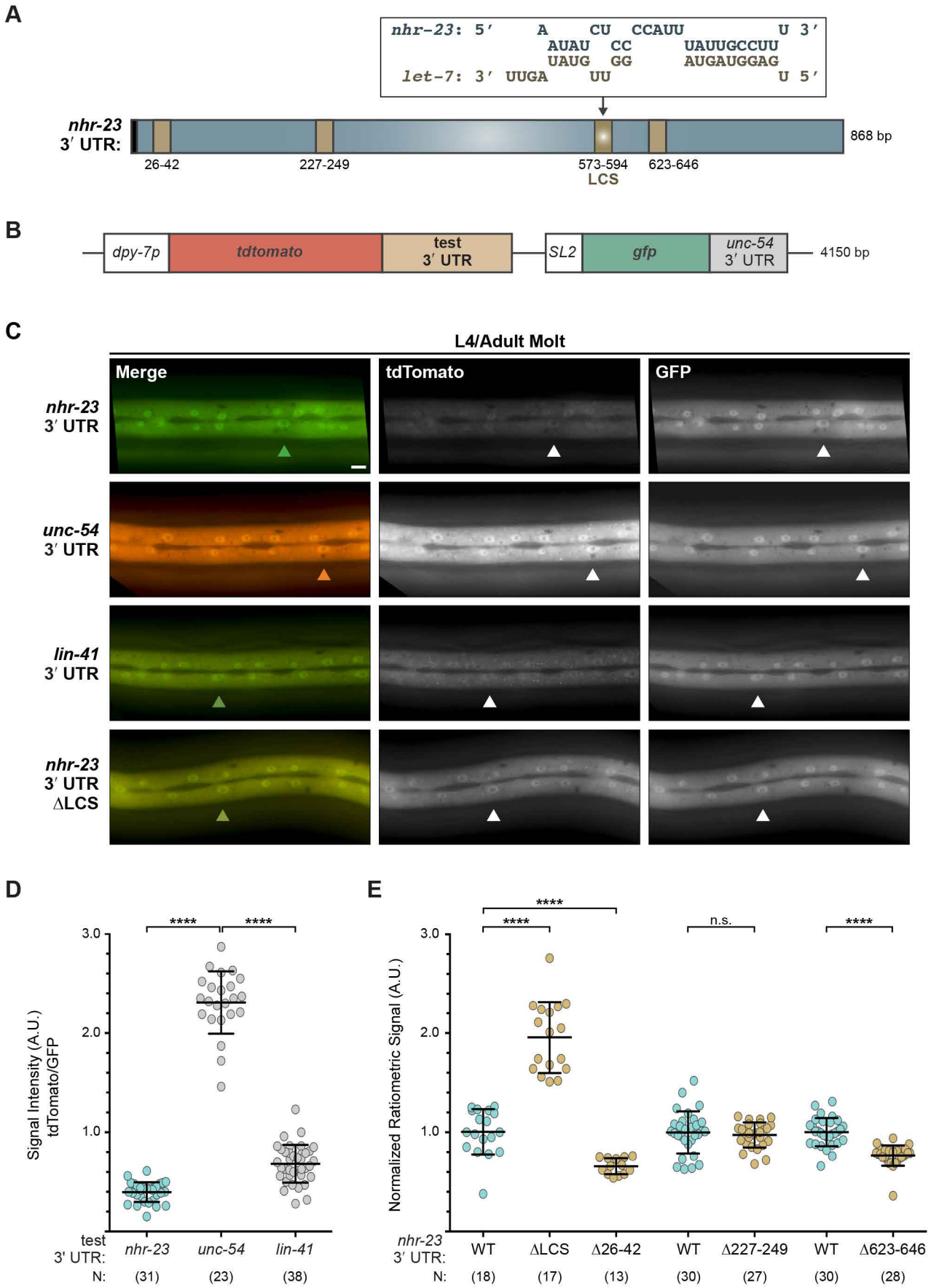
A
nhr-23: 5′ A CU CCAUU U 3′
AUAU CC UAUUGCCUU
UAUG GG AUGAUGGAG
let-7: 3′ UUGA UU U 5′
nhr-23 3′ UTR:
868 bp
26-42
227-249
573-594
LCS
623-646
B
dpy-7p
tdtomato
test 3′ UTR
SL2
gfp
unc-54 3′ UTR
4150 bp
C
L4/Adult Molt
Merge
tdTomato
GFP
nhr-23 3′ UTR
unc-54 3′ UTR
lin-41 3′ UTR
nhr-23 3′ UTR ΔLCS
D
Signal Intensity (A.U.) tdTomato/GFP
test 3′ UTR:
nhr-23
unc-54
lin-41
N:
(31)
(23)
(38)
E
Normalized Ratiometric Signal (A.U.)
nhr-23 3′ UTR:
WT
ΔLCS
Δ26-42
WT
Δ227-249
WT
Δ623-646
N:
(18)
(17)
(13)
(30)
(27)
(30)
(28)
n.s.

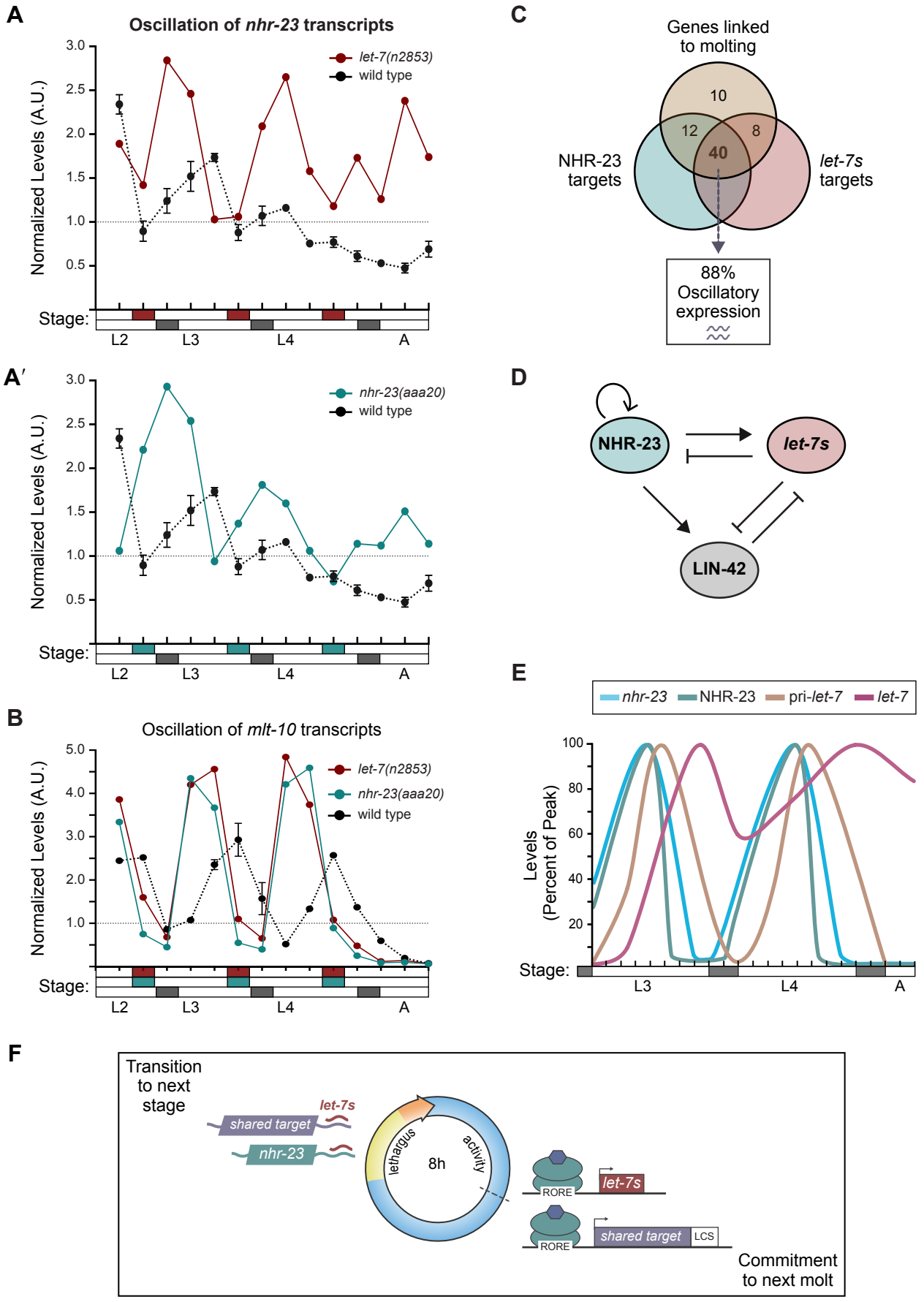
A
Oscillation of nhr-23 transcripts
let-7(n2853)
wild type
Normalized Levels (A.U.)
Stage:
L2
L3
L4
A
A′
nhr-23(aaa20)
wild type
B
Oscillation of mlt-10 transcripts
let-7(n2853)
nhr-23(aaa20)
wild type
C
Genes linked to molting
10
12
8
40
NHR-23 targets
let-7s targets
88% Oscillatory expression
D
NHR-23
let-7s
LIN-42
E
nhr-23
NHR-23
pri-let-7
let-7
Levels (Percent of Peak)
F
Transition to next stage
let-7s
shared target
nhr-23
lethargus
activity
8h
RORE
let-7s
shared target
LCS
Commitment to next molt

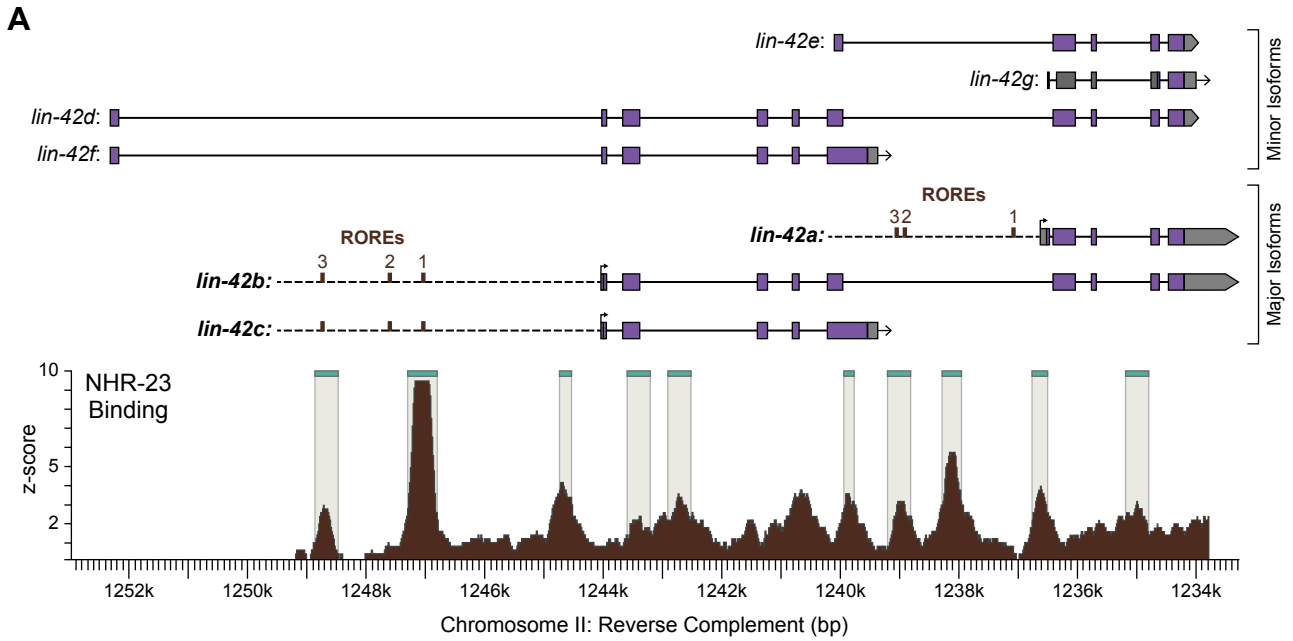
A
lin-42e:
lin-42g:
lin-42d:
lin-42f:
Minor Isoforms
RORES
3 2 1
lin-42a:
RORES
3 2 1
lin-42b:
lin-42c:
Major Isoforms
NHR-23
Binding
z-score
10
5
2
1252k
1250k
1248k
1246k
1244k
1242k
1240k
1238k
1236k
1234k
Chromosome II: Reverse Complement (bp)

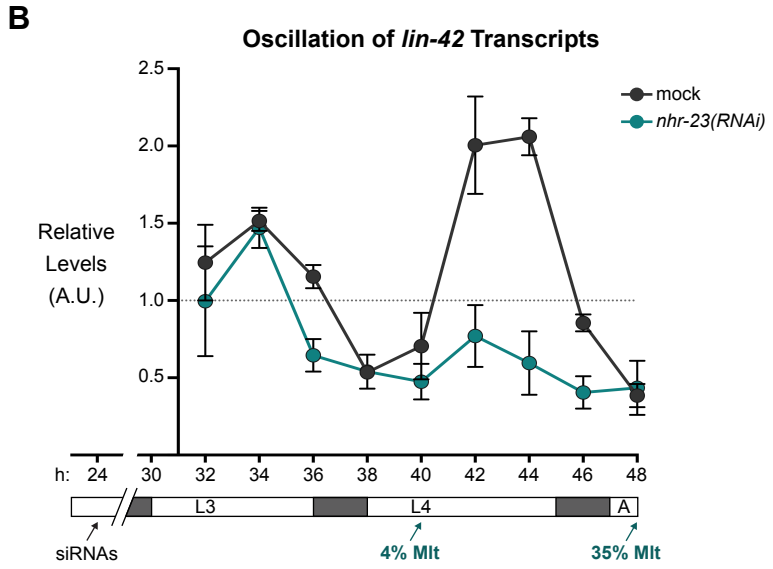
B
Oscillation of lin-42 Transcripts
mock
nhr-23(RNAi)
Relative
Levels
(A.U.)
2.5
2.0
1.5
1.0
0.5
h: 24 30 32 34 36 38 40 42 44 46 48
L3
L4
A
siRNAs
4% Mlt
35% Mlt

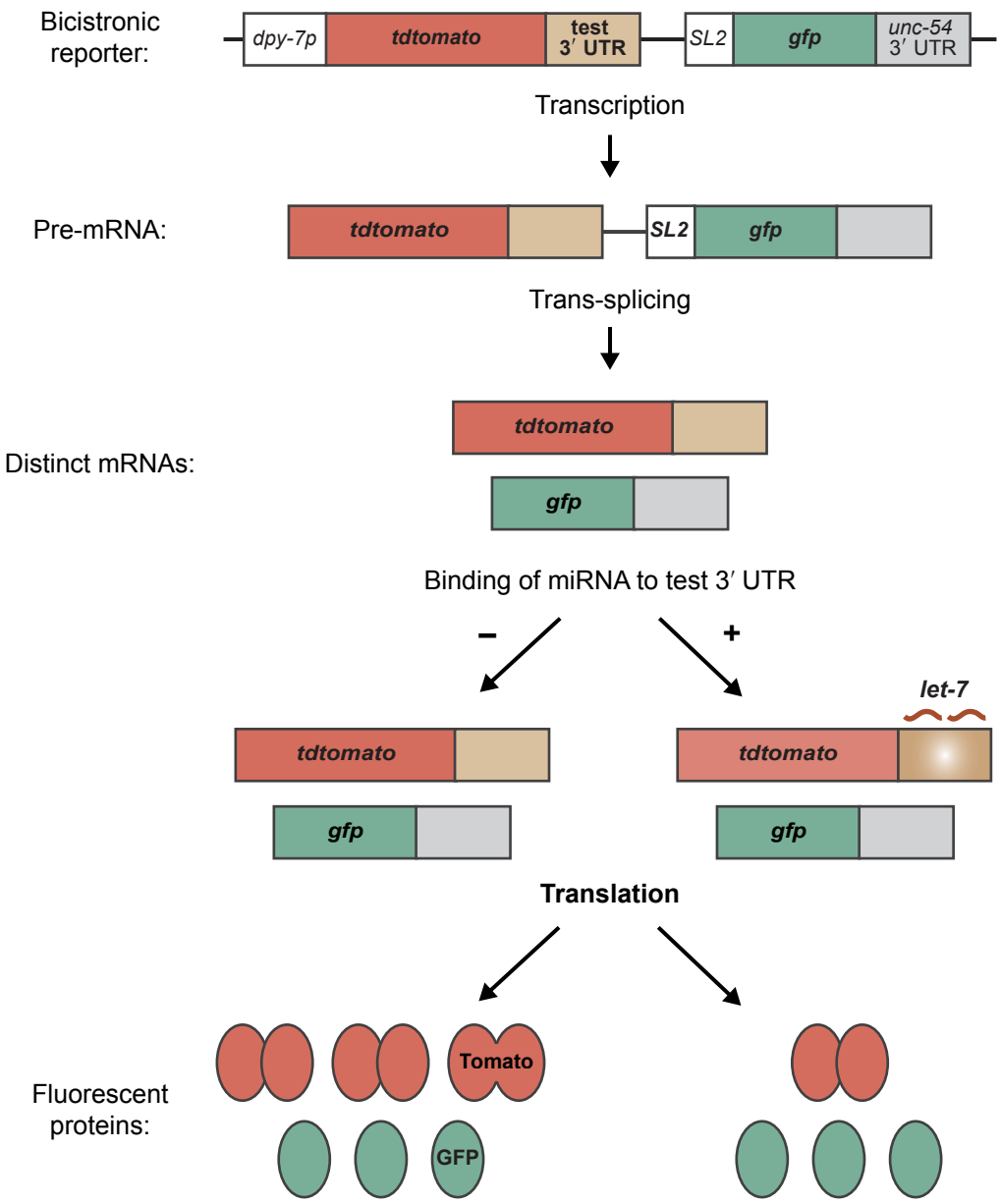
Bicistronic reporter:
dpy-7p
tdtomato
test 3′ UTR
SL2
gfp
unc-54 3′ UTR
Transcription
Pre-mRNA:
tdtomato
SL2
gfp
Trans-splicing
Distinct mRNAs:
tdtomato
gfp
Binding of miRNA to test 3′ UTR
–
+
let-7
tdtomato
gfp
tdtomato
gfp
Translation
Fluorescent proteins:
Tomato
GFP

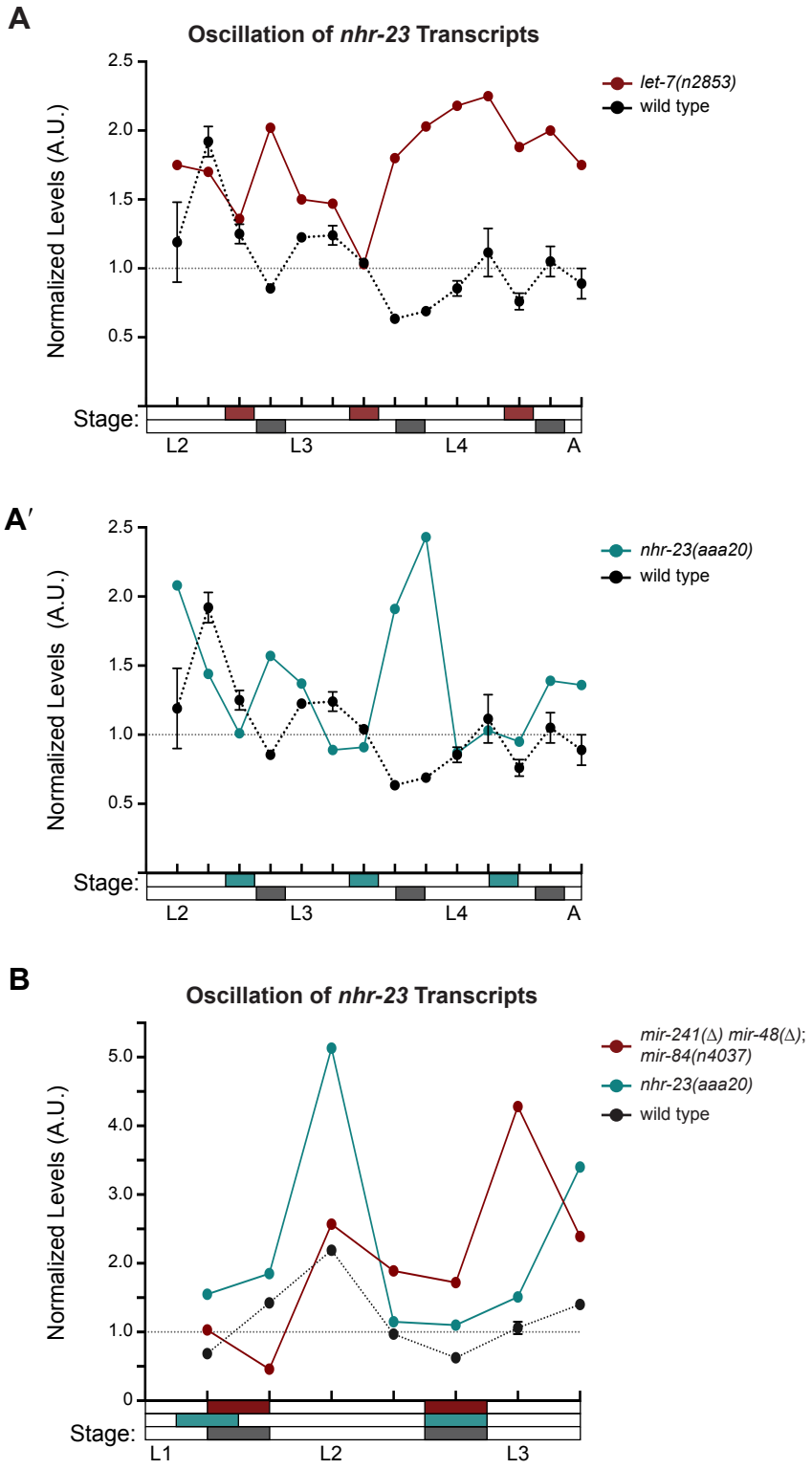
A
Oscillation of nhr-23 Transcripts
Normalized Levels (A.U.)
2.5
2.0
1.5
1.0
0.5
let-7(n2853)
wild type
Stage:
L2
L3
L4
A
A′
Normalized Levels (A.U.)
nhr-23(aaa20)
wild type
Stage:
L2
L3
L4
A
B
Oscillation of nhr-23 Transcripts
Normalized Levels (A.U.)
5.0
4.0
3.0
2.0
1.0
0
mir-241(Δ) mir-48(Δ); mir-84(n4037)
nhr-23(aaa20)
wild type
Stage:
L1
L2
L3

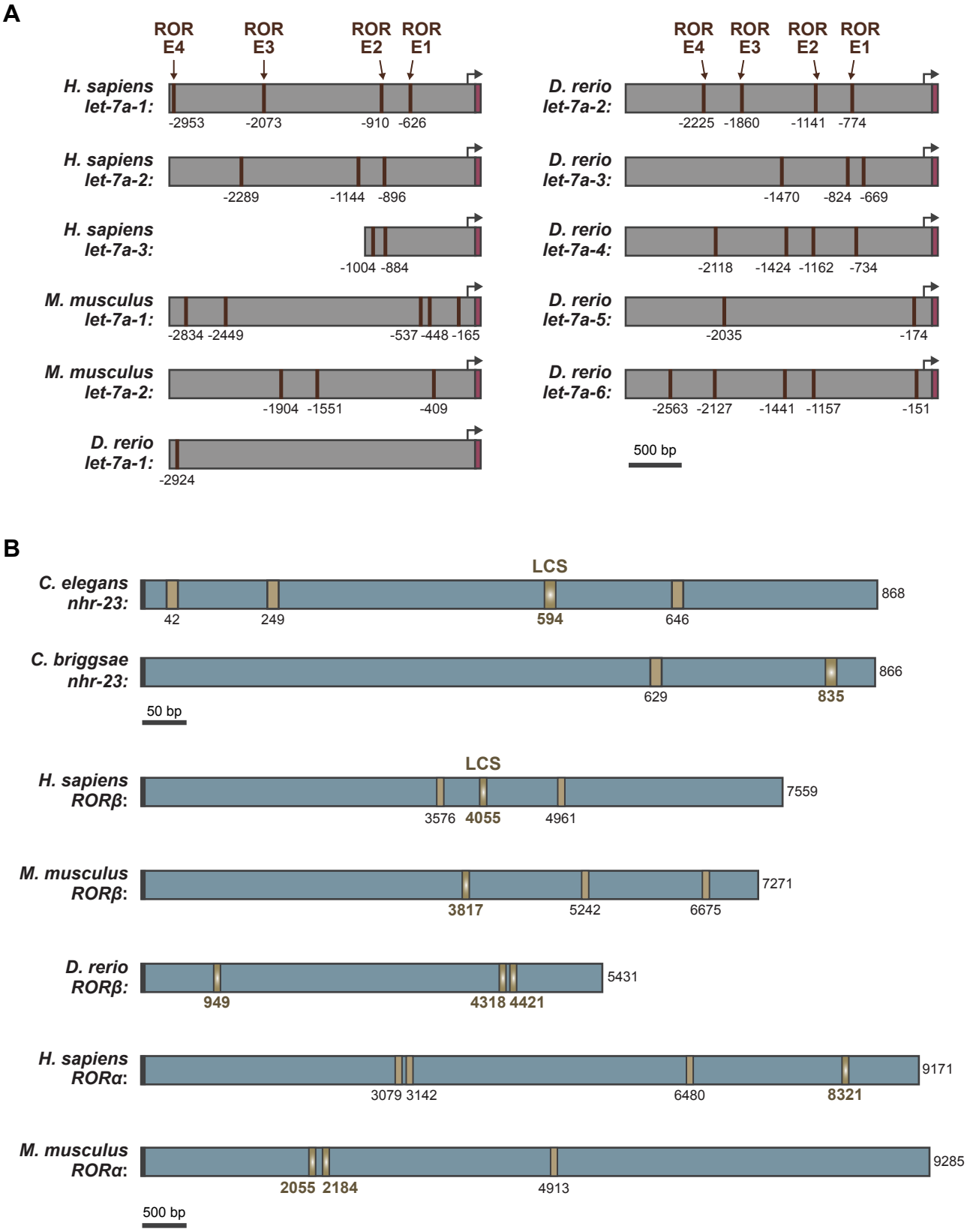
A
ROR E4
ROR E3
ROR E2
ROR E1
H. sapiens let-7a-1:
-2953 -2073 -910 -626
H. sapiens let-7a-2:
-2289 -1144 -896
H. sapiens let-7a-3:
-1004 -884
M. musculus let-7a-1:
-2834 -2449 -537 -448 -165
M. musculus let-7a-2:
-1904 -1551 -409
D. rerio let-7a-1:
-2924
D. rerio let-7a-2:
-2225 -1860 -1141 -774
D. rerio let-7a-3:
-1470 -824 -669
D. rerio let-7a-4:
-2118 -1424 -1162 -734
D. rerio let-7a-5:
-2035 -174
D. rerio let-7a-6:
-2563 -2127 -1441 -1157 -151
500 bp
B
LCS
C. elegans nhr-23:
42 249 594 646 868
C. briggsae nhr-23:
629 835 866
50 bp
LCS
H. sapiens RORβ:
3576 4055 4961 7559
M. musculus RORβ:
3817 5242 6675 7271
D. rerio RORβ:
949 4318 4421 5431
H. sapiens RORα:
3079 3142 6480 8321 9171
M. musculus RORα:
2055 2184 4913 9285
500 bp

Supplemental Table 1 – Relates to Figure 1. Comparative Metrics of Molting Biorhythms

		Interval (h)												
		Active				Lethargic				Wake-to-Wake				
L2 to L3														
RNAi	**Strain**	mean	sd	cv	p	mean	sd	cv	p	mean	sd	cv	n	p
–	wild type	5.9	0.3	0.05	–	1.3	0.5	0.36	–	7.2	0.4	0.06	18	–
nhr-23	wild type	6.1	0.6	0.10	n.s.	3.9	1.1	0.28	****	9.9	1.0	0.10	19	****
–	*mir-41Δ mir-241Δ; mir-84(n4037)*	6.3	0.7	0.11	n.s.	1.3	0.5	0.36	n.s.	7.6	0.7	0.10	17	n.s.
nhr-23	*mir-41Δ mir-241Δ; mir-84(n4037)*	6.4	0.8	0.13	n.s.	3.0	0.4	0.13	****	9.4	0.8	0.09	15	****
L3 to L4														
RNAi	**Strain**	mean	sd	cv	p	mean	sd	cv	p	mean	sd	cv	n	p
–	wild type	6.3	0.4	0.07	–	1.6	0.5	0.31	–	7.9	0.7	0.08	17	–
nhr-23	wild type	7.7	1.2	0.15	****	3.8	1.9	0.49	****	11.4	1.9	0.16	12	****
–	*let-7(n2853)*†	5.6	0.6	0.11	*	1.3	0.4	0.36	n.s.	6.8	0.5	0.07	18	*
nhr-23	*let-7(n2853)*	5.8	0.8	0.13	n.s.	3.8	0.6	0.17	****	9.6	0.9	0.09	18	****
L4 to Adult														
RNAi	**Strain**	mean	sd	cv	p	mean	sd	cv	p	mean	sd	cv	n	p
–	wild type	8.1	0.5	0.06	–	2.2	0.4	0.18	–	10.3	0.4	0.05	16	–
nhr-23	wild type	8.4	0.8	0.09	n.s.	4.6	0.7	0.16	****	13.0	1.1	0.08	17	****
–	*let-7(n2853)*†	6.7	0.6	0.09	****	1.6	0.5	0.30	**	8.4	0.6	0.07	17	****
–	*let-7(n2853)*	6.3	0.4	0.08	****	1.5	0.5	0.33	*	7.9	0.6	0.08	15	****
nhr-23	*let-7(n2853)*	6.7	0.6	0.10	****	3.9	0.6	0.16	****	10.6	0.8	0.07	19	n.s.
–	wild type	7.8	0.5	0.07	–	2.2	0.6	0.18	–	10.0	0.5	0.05	20	–
–	*let-7(mg279)*	7.2	0.6	0.08	**	2.2	0.4	0.17	n.s.	9.3	0.6	0.06	20	**
–	*let-7(mg279) mir-84(tm1304)*	6.1	0.9	0.15	****	2.4	0.6	0.25	n.s.	8.5	0.9	0.15	18	****

†Values for one cohort of animals, which is depicted in Figure 1B′.

Supplemental Table 2 – Relates to Figure 3 and Supplemental Figure 4. LCSs found in nematode and vertebrate homologs of *ROR*

Species	Gene	Identifier	3' UTR length*	LCS 3' nt.	TS (kcal/mol)	Alignment (target 3' UTR versus *let-7*)
C. elegans	*nhr-23*	NM_001025806	868	42	-21.8	5' UU C UG – – C 3' UUAU CA CU CU CCUU GAUA GU GA GA GGAG 3' UU U UG U U U 5'
				249	-15.2	5' U U GAG G U 3' G CUG UGCAG A U CCUCA U GAU AUGUU U A GGAGU 3' U – GGA G U 5'
				594	-17.0	5' UUAA CU CCAUU U 3' AUAU CC UAUUGCCUU UAUG GG AUGAUGGAG 3' UUGA UU ----- U 5'
				646	-17.6	5' C UUAAU – UC – U 3' GCU UAC GCCU UUACC CA UGA AUG UGGA GAUGG GU 3' U U---- U U– A 5'
C. briggsae	*nhr-23*	WBGene 00040598	866	629	-20.7	5' UU C CGCU U C 3' C AUACAACU CUGC CUC G UAUGUUGG GAUG GAG 3' UU A AU-- – U 5'
				835	-21.8	5' UUAC CUUUUUU C 3' AUAUAAUCU CUGCCUC UAUGUUGGA GAUGGAG 3' UUGA U------ U 5'
H. sapiens	*RORβ*	NM_006914	7559	3576	-25.9	5' CGC – C 3' GGCU UGCAAUCU CUGCCUC UUGA AUGUUGGA GAUGGAG 3' U-- U U 5'
				4055	-23.1	5' U A UUU AUCAUA G 3' G C GUACA CCU GCUGCCUU U G UAUGU GGA UGAUGGAG 3' U A U-- ------ U 5'
				4961	-23.1	5' C – A U 3' GAU GU CAGCUUGC GCCUC UUG UA GUUGGAUG UGGAG 3' A U A U 5'
M. musculus	*RORβ*	NM_146095	7271	3817	-23.8	5' A GC CU U 3' GG UG CAACU UACUGCCUC UU AU GUUGG AUGAUGGAG 3' G AU -- U 5'
				5242	-22.7	5' GUCACA GAUGCUUC G 3' AACUA GCAACC CUGCCU UUGAU UGUUGG GAUGGA 3' A----- AU------ GU 5'
				6675	-26.7	5' AG – C 3' GA GUACAGCUUGCU CCUC UU UAUGUUGGAUGA GGAG 3' GA U U 5'
D. rerio	*RORβ*	NM_001082856	5431	949	-21.8	5' AA C U– U 3' U AUAU UCUGCUGCCUU G UAUG GGAUGAUGGAG 3' UU A UU U 5'
				4318	-23.8	5' U AAAAUAAA G 3' A UUGUACA GCU ACUACUUCA U GAUAUGU UGG UGAUGGAGU 3' U -------- A 5'
				4421	-23.3	5'U ACACAGGCAAACA AUCA U 3' GCUAUAU GAC UACUGCCUU UGAUAUG UUG AUGAUGGAG 3'U ---------- G--- U 5'
H. sapiens	*RORα*	NM_134261	9171	3079	-23.7	5' C – CC A 3' ACUGU CAGCC GCUGCU CA UGAUA GUUGG UGAUGG GU 3' U U A– A 5'
				3142	-22.8	5' UU AA AA C 3' UUGUACA GCCUG UACCUU GAUAUGU UGGAU AUGGAG 3' UU -- G– U 5'
				6480	-24.0	5' C UGUCU – U 3' A CUGUAU GCCUGCU CCUU U GAUAUG UGGAUGA GGAG 3' U U---- U U 5'
				8321	-22.2	5' U AAUC UCAUU UA U 3' A ACA CCU ACUGCCUC U UGU GGA UGAUGGAG 3' U GAUA U---- -- U 5'
M. musculus	*RORα*	NM_013646	9285	2055	-23.9	5' CC C A C 3' CJ AUGUA CC GCUGCCUC GAUAUGU GG UGAUGGAG 3' UU U A U 5'
				2184	-23.7	5' U U U 3' AACU UAC GACUU CUGCCUUA UUGA AUG UUGGA GAUGGAGU 3' U U 5'
				4913	-22.6	5' C A CAUC G C 3' AC GUGCAGCC UGCUG CUU UG UAUGUUGG AUGAU GAG 3' U A ---- G U 5'

*3' UTRs were supported by ESTs archived in WBcel235/ce11, WBPS9, GRCh38/hg38, GRCm38/mm10, and GRCz10/danRer10.

Supplemental Table 3 – Relates to Figure 4. Classification of genes linked to molting as targets of NHR-23, *let-7s*, neither or both.

Gene Name	Sequence	Criteria for targets of NHR-23:					NHR-23 target (Y/N)	Criteria for targets of *let-7s*:				*let-7s* target (Y/N)	Target class	Cyclic mRNA levels (≈)
		Size of upstream regulatory region & first intron (kb)	ROREs #	ROREs # Obs. / # Exp.	mRNA levels after *nhr-23* RNAi	NHR-23 ChIP-Seq Peaks (#)		Size of 3' UTR (nt.)	LCSs #	LCSs # Obs. / # Exp.	ALG-1 iCLIP Peaks (+/-)			
Potential Clock Components														
let-7	C05G5.6	1.5	3	5.8	↓	1	Y	N/A	–	–	–	N/A	NHR-23	≈
lin-42a	F47F6.1	3.7	3	2.3	↓	4	Y	939	4	3.2	+	Y	Shared	≈
lin-42b	F47F6.1	5.5	3	1.6	↓	3	Y	939	4	3.2	+	Y	Shared	≈
lin-42c	F47F6.1	5.5	3	1.6	↓	3	Y	156	0	0	–	N	NHR-23	≈
mir-48	F56A12.3	1.7	2	3.4	–	1	Y	N/A	–	–	–	N/A	NHR-23	≈
mir-241	F56A12.4	2.0	2	2.9	–	2	Y	N/A	–	–	–	N/A	NHR-23	≈
mir-84	B0395.4	2.8	1	1.1	–	2	Y	N/A	–	–	–	N/A	NHR-23	≈
nhr-23	C01H6.5	6.1	8	3.8	↓	3	Y	868	3	2.6	+	Y	Shared	≈
nhr-25	F11C1.6	6.9	3	1.3	–	3	Y	749	1	1.0	+	Y	Shared	≈
Gene Regulatory Factors														
alg-1	F48F7.1	9.9	11	3.2	–	3	Y	400	1	1.9	+	Y	Shared	≈
bed-3	F25H8.6	1.7	2	3.4	–	1	Y	459	1	1.6	+	Y	Shared	≈
blmp-1	F25D7.3	6.7	7	3.0	–	4	Y	861	3	2.6	+	Y	Shared	≈
bro-1	F56A3.5	1.2	0	0.0	–	1	N	379	1	2.0	–	N	–	≈
dre-1	K04A8.6	7.5	8	3.1	–	4	Y	376	2	4.0	+	Y	Shared	≈
mab-10	R166.1	6.0	8	3.9	–	2	Y	374	1	2.0	–	N	NHR-23	≈
nhr-41	Y104H12A.1	11.1	23	6.0	–	2	Y	332	1	2.3	–	N	NHR-23	≈
nhr-67	C08F8.8	5.5	5	2.6	–	0	N	241	3	9.5	–	N	–	–
pqn-47	F59B10.1	5.9	7	3.4	–	5	Y	804	2	1.9	+	Y	Shared	≈
rnt-1	B0414.2	9.2	4	1.3	–	0	N	221	0	0	–	N	–	≈
daf-12	F11A1.3	17.0	12	2.0	–	7	Y	1393	5	2.7	+	Y	Shared	–
gei-8	C14B9.6	1.8	1	1.6	–	3	Y	449	4	6.7	+	Y	Shared	–
skn-1	T19E7.2	5.1	2	1.1	–	2	Y	677	1	1.1	+	Y	Shared	–
Signaling Pathway Components														
acn-1	C42D8.5	4.0	4	2.9	↓	3	Y	384	1	2.0	+	Y	Shared	≈
apl-1	C42D8.8	4.9	4	2.4	–	5	Y	678	1	1.1	+	Y	Shared	≈
calu-1	M03F4.7	1.7	3	5.1	–	3	Y	256	1	3.0	+	Y	Shared	≈
cki-1	T05A6.1	1.9	2	3.1	–	1	Y	235	2	6.5	+	Y	Shared	≈
daf-9	T13C5.1	1.1	0	0.0	↓	1	Y	214	2	7.2	+	Y	Shared	–
glf-1	H04M03.4	2.4	1	1.2	↓	1	Y	247	2	6.2	–	N	NHR-23	≈
lin-3	F36H1.4	5.5	5	1.9	–	0	N	442	5	8.5	+	Y	*let-7s*	–
let-767	C56G2.6	0.6	1	4.8	–	1	Y	87	1	9.2	+	Y	Shared	–
lon-1	F48E8.1	4.8	3	1.8	–	5	Y	185	2	8.3	+	Y	Shared	≈
lrp-1	F29D11.1	7.9	3	1.1	–	6	Y	346	2	4.4	+	Y	Shared	≈
mlt-8	W08F4.6	3.5	2	1.7	↓	1	Y	270	2	5.6	+	Y	Shared	≈
nekl-2	ZC581.1	1.1	1	2.6	–	0	N	73	0	0	–	N	–	≈
nlp-22	T24D8.3	0.8	0	0.0	–	0	N	1000	2	1.5	–	N	–	≈
osm-7	T05D4.4	3.5	1	0.8	–	0	N	121	1	6.5	+	Y	*let-7s*	≈
osm-11	F11C7.5	2.8	1	1.1	–	3	Y	545	4	5.5	+	Y	Shared	≈
phi-59	T19B10.2	1.5	0	0.0	↓	1	Y	121	1	6.5	+	Y	Shared	≈
pod-2a	W09B6.1	3.0	4	3.9	–	2	Y	324	1	2.3	–	N	NHR-23	≈
ptr-4	C45B2.7	4.5	4	2.6	↓	2	Y	221	2	6.9	–	N	NHR-23	≈
ptr-23	ZK270.1	2.0	0	0.0	–	2	N	311	3	7.3	+	Y	*let-7s*	≈
qua-1	T05C12.10	5.7	3	1.5	↓	4	Y	340	1	2.2	+	Y	Shared	≈
	E03H4.8	3.4	1	0.9	–	0	N	307	1	2.5	–	N	–	≈
	T19A5.3	4.9	2	1.2	↓	2	Y	347	1	2.2	+	Y	Shared	≈
	Y47D3B.1	4.9	3	1.8	–	1	Y	98	1	8.1	–	N	NHR-23	≈
Extracellular Matrix Proteins and Receptors														
adt-2	F08C6.1	7.6	7	2.7	–	6	Y	621	1	1.2	+	Y	Shared	≈
bli-5	F45G2.5	1.4	0	0.0	–	0	N	300	1	2.5	+	Y	*let-7s*	≈
bus-8	T23F2.1	3.6	0	0.0	↓	0	N	453	2	3.3	–	N	–	≈
clc-1	C09F12.1	5.4	0	0.0	–	0	N	101	1	7.8	–	N	–	≈

col-12	F15H10.1	0.7	0	0.0	–	0	N	101	1	7.8	+	Y	*let-7s*	≈
dpy-13	F30B5.1	3.8	5	3.8	–	4	Y	63	2	26.1	+	Y	Shared	≈
dpy-17	F54D8.1	0.4	1	7.3	–	0	N	54	1	15.5	–	N	–	≈
dpy-4	Y41E3.2	2.4	0	0.0	–	1	N	102	1	7.8	+	Y	*let-7s*	≈
dpy-5	F27C1.8	0.8	1	3.6	↓	1	Y	39	0	0	–	N	NHR-23	≈
dpy-7	F46C8.6	0.7	2	8.3	↓	1	Y	236	1	3.2	–	N	NHR-23	≈
fbn-1	ZK783.1	8.3	12	4.2	↓	6	Y	457	1	1.7	+	Y	Shared	≈
ina-1	Y116A8A.9	8.0	8	2.9	–	2	Y	261	1	2.9	+	Y	Shared	≈
mam-1	ZC13.3	3.8	3	2.3	–	0	N	243	0	0	–	N	–	≈
mlt-10	C09E8.3	8.6	4	1.3	↓	1	Y	139	2	11.2	+	Y	Shared	≈
mlt-11	W01F3.3	5.2	11	6.1	↓	4	Y	353	1	2.1	+	Y	Shared	≈
mlt-7	ZK430.8	11.5	15	3.8	–	1	Y	317	2	4.8	+	Y	Shared	≈
mlt-9	F09B12.1	3.5	1	0.8	↓	5	Y	313	1	2.4	–	N	NHR-23	≈
mup-4	K07D8.1	5.8	5	2.5	–	2	Y	394	0	0	–	N	NHR-23	≈
nas-36	C26C6.3	1.1	1	2.6	↓	0	Y	327	5	11.6	+	Y	Shared	≈
nas-37	C17G1.6	3.6	7	5.6	↓	2	Y	240	4	12.7	–	N	NHR-23	≈
noah-1	C34G6.6	7.9	9	3.3	↓	5	Y	550	1	1.4	+	Y	Shared	≈
noah-2	F52B11.3	8.9	3	1.0	↓	6	Y	316	2	4.8	+	Y	Shared	≈
pan-1	M88.6	2.5	2	2.3	–	2	Y	393	2	3.8	+	Y	Shared	≈
pat-2	F54F2.1	4.0	4	2.9	–	2	Y	292	2	5.2	+	Y	Shared	≈
rol-6	T01B7.7	3.4	2	1.7	↓	4	Y	117	1	6.7	+	Y	Shared	≈
pat-3	ZK1058.2	5.0	0	0.0	–	2	N	400	1	1.9	+	Y	*let-7s*	≈
Cytoskeletal Components														
ifa-2	W10G6.3	1.7	1	1.7	–	1	Y	186	2	8.3	–	N	Shared	≈
ifc-2	M6.1	3.0	0	0.0	–	0	N	536	2	2.8	+	Y	*let-7s*	≈
nmy-2	F20G4.3	1.8	6	9.7	–	1	Y	448	2	3.4	+	Y	Shared	≈
Randomly Selected Genes with no Known Link to Molting														
acs-13	Y65B4BL.5	4.9	3	1.8	–	2	Y	424	1	1.8	+	Y	Shared	–
ced-8	F08F1.5	0.7	0	0.0	–	0	N	85	0	0	–	N	–	–
cyp-33C12	Y5H2B.6	1.5	0	0.0	–	0	N	148	0	0	–	N	–	–
ech-5	F56B3.5	0.5	0	0.0	–	1	N	602	1	1.2	–	N	–	–
map-2	Y116A8A.9	1.5	1	1.9	–	0	N	274	2	5.6	–	N	–	–
mpst-7	R186.6	1.0	0	0.0	–	1	N	84	0	0	+	N	–	–
nhr-176	F14H3.11	0.2	0	0.0	–	0	N	54	1	15.5	–	N	–	–
nlp-37	F48B9.4	2.9	3	3.0	–	0	N	302	2	5	–	N	–	–
srz-10	ZK1037.11	1.1	1	2.6	–	0	N	16	0	0	–	N	–	–
slc-36.5	C44B7.6	2.4	3	3.6	–	1	Y	74	0	0	–	N	NHR-23	≈
ttll-12	D2013.9	0.1	0	0.0	–	0	N	175	1	4.4	+	Y	*let-7s*	–
unc-112	C47E8.7	2.8	1	1.1	–	1	Y	295	1	2.6	+	Y	Shared	–
	C01G6.9	0.1	0	0.0	–	0	N	76	1	10.6	–	N	–	–
	C06E1.7	2.4	1	1.2	–	1	Y	151	3	15.4	–	N	NHR-23	≈
	F44E5.5	0.4	0	0.0	–	1	N	39	0	0	–	N	–	–
	R10E8.6	1.3	0	0.0	–	0	N	31	0	0	–	N	–	–
	R12B2.2	0.5	0	0.0	–	0	N	115	0	0	–	N	–	–
	T06D4.1	2.3	3	3.8	–	0	N	234	0	0	–	N	–	–
	T19D12.4	2.3	0	0.0	–	0	N	115	0	0	–	N	–	≈
	Y53C10A.6	6.3	0	0.0	–	0	N	201	2	7.6	–	N	–	–